REPORT 1305

MEASUREMENT OF AERODYNAMIC FORCES FOR VARIOUS MEAN ANGLES OF ATTACK ON AN AIRFOIL OSCILLATING IN PITCH AND ON TWO FINITE-SPAN WINGS OSCILLATING IN BENDING WITH EMPHASIS ON DAMPING IN THE STALL [1]

By A. Gerald Rainey

SUMMARY

The oscillating air forces on a two-dimensional wing oscillating in pitch about the midchord have been measured at various mean angles of attack and at Mach numbers of 0.35 and 0.7. The magnitudes of normal-force and pitching-moment coefficients were much higher at high angles of attack than at low angles of attack for some conditions. Large regions of negative damping in pitch were found, and it was shown that the effect of increasing the Mach number from 0.35 to 0.7 was to decrease the initial angle of attack at which negative damping occurred.

Measurements of the aerodynamic damping of a 10-percent-thick and of a 3-percent-thick finite-span wing oscillating in the first bending mode indicate no regions of negative damping for this type of motion over the range of variables covered. The damping measured at high angles of attack was generally larger than that at low angles of attack.

INTRODUCTION

Recently, the problems of stall flutter and buffeting have been the subjects of several analytical investigations. (See refs. 1 to 8.) These studies have indicated some interesting approaches to the dynamic problems associated with separated flow; however, because of the great difficulty in treating the unsteady aerodynamics of wings with separated flow, a completely satisfactory analytical approach has not been developed. Therefore, additional experimental information is required in order to describe further the phenomena of stall flutter and buffeting.

It is generally accepted that, when a wing is sufficiently stalled, fluctuating forces act on the wing and, if the wing is flexible, it will respond to these forces. If the total damping of the system remains positive, the characteristics of the response will depend in part on the characteristics of the fluctuating forcing function, and the amount the wing responds will depend on the relative magnitudes of the forcing function and the damping. This phenomenon may serve as a rather general description of buffeting.

If, on the other hand, the damping becomes negative, the characteristics and amount of the response will depend primarily on the character of the damping, that is, on the degree of nonlinearity. This latter case describes the phenomenon of stall flutter. Then, in essence, the phenomena of stall flutter and buffeting, as defined herein, differ primarily in the sign of the damping. Consequently, knowledge of the conditions under which the aerodynamic damping becomes negative is essential in order to decide on the proper approach to the problem.

The purpose of this report is to present the results of two somewhat different investigations both of which were intended to provide additional information concerning the conditions under which aerodynamic damping may become negative, as well as some quantitative information concerning the amount of aerodynamic damping. In addition, the techniques and instrumentation employed are given in some detail. The first part of this report deals with the results of some measurements of oscillating normal forces and pitching moments for an NACA 65A010 airfoil oscillating in pitch about the midchord. Some additional results obtained with this pitching airfoil with two different types of disturbances at the leading edge are presented in appendix A. The second part gives the results of measurements of aerodynamic damping for two different finite-span wings oscillating in essentially the first bending mode.

SYMBOLS

a_1	tip deflection in first bending mode, ft
c	wing chord, ft
c_r	reference wing chord at three-quarter semispan, ft
C	structural damping per unit length, lb-sec/ft^2
C_{cr}	critical value of damping, lb-sec/ft
C_a	effective value of aerodynamic damping, lb-sec/ft
C_s	effective value of structural damping, lb-sec/ft
c_m	section pitching-moment coefficient about midchord
$\left\lvert\frac{dc_m}{d\alpha}\right\rvert$	absolute magnitude of fundamental component of oscillating section pitching-moment coefficient about midchord per radian
c_n	section normal-force coefficient
$\left\lvert\frac{dc_n}{d\alpha}\right\rvert$	absolute magnitude of fundamental component of oscillating section normal-force coefficient per radian
EI	bending rigidity, lb-ft^2
f	frequency, cps
F	total applied force acting on finite-span wing, lb

[1] Supersedes NACA Technical Note 3643 by A. Gerald Rainey, 1956.

F_e effective value of aerodynamic-damping coefficient for finite-span wing oscillating in bending mode (eq. (3))

h vertical deflection of equivalent spring-mass system, ft

$h_1(y)$ first-bending-mode shape expressed in terms of unit tip deflection

k reduced frequency, $\omega c/2V$

K_c effective spring constant of wire, coil, and spring attached to finite-span models, lb/ft

K_e spring constant of equivalent spring-mass system, lb/ft

K_{h_1} beam stiffness in first bending mode, lb/ft

L length of semispan models, ft

m mass per unit length, lb-sec^2/ft^2

$|M|$ absolute magnitude of fundamental component of oscillatory aerodynamic pitching moment about midchord, ft-lb

M_c effective mass of wire, coil, and spring attached to finite-span models, lb-sec^2/ft

ΔM_c increment of coil mass, lb-sec^2/ft

M_e mass of equivalent spring-mass system, lb-sec^2/ft

M_{h_1} beam mass in first bending mode, lb-sec^2/ft

$M(t)$ total oscillatory pitching moment indicated by pressure-gage integrator, ft-lb

M_{01} part of pitching-moment signal passed by filter which is definitely related in phase to the motion, ft-lb

ΔM_R part of pitching-moment signal passed by filter which is not correlated with the motion, ft-lb

N aerodynamic and exciting forces normal to finite-span wings

$|N|$ absolute magnitude of fundamental component of oscillatory aerodynamic normal force, lb

$N(t)$ total oscillatory normal force indicated by pressure-gage integrator, lb

N_{01} part of normal-force signal passed by filter which is directly related in phase to the motion, lb

ΔN_R part of normal-force signal passed by filter which is correlated with the motion, lb

Δp incremental pressure acting between upper and lower surface of wing, lb/sq ft

S wing area, sq ft

T arbitrary period of time, sec

t time, sec

V flow velocity, ft/sec

y spanwise coordinate, ft

y_c spanwise coordinate at point of attachment of wire-spring-shaker-coil system, ft

α instantaneous angle of attack, radians

$|\alpha|$ absolute magnitude of fundamental component of oscillatory angle of attack, deg (except when used in defining oscillatory derivatives)

$\bar{\alpha}$ mean angle of attack about which oscillation occurs, deg

α_{01} part of angle-of-attack signal passed by filter which is directly related in phase to normal force or pitching moment

κ_e effective value of mass-ratio parameter

ρ mass density of test medium, lb-sec^2/ft^4

ϕ_m phase angle by which pitching moment leads the motion, deg

ϕ_n phase angle by which normal force leads the motion, deg

ω circular frequency, $2\pi f$, radians/sec

ω_1 first natural frequency, radians/sec

ω_{1_Δ} first natural frequency of wing-shaker system with added mass, radians/sec

Subscripts:

0 quantities which have same frequency and which are directly related in phase to sinusoidal forces or motions

R quantities which are not correlated with sinusoidal forces or motions

Bars indicate an average with respect to time.

One dot indicates first derivative with respect to time, and two dots indicate second derivative with respect to time.

TWO-DIMENSIONAL AIRFOIL OSCILLATING IN PITCH ABOUT MIDCHORD

TECHNIQUE

The normal forces and pitching moments acting on an NACA 65A010 airfoil oscillating in pitch about the midchord at high mean angles of attack were measured by use of a technique involving an electrical pressure-gage integrator. Some of the methods and instrumentation used have been briefly described in reference 9 wherein results are presented of measurements of oscillating air forces at a mean angle of attack of zero. For this condition, the instrumentation and methods presented in reference 9 were considered to be adequate; but, when measurements were undertaken at mean angles of attack beyond the stall, it was found that relatively large random forces existed and somewhat different instrumentation and data-reduction procedures were required in order to obtain the desired quantities. A detailed description of the apparatus, testing procedures, and methods of reducing the data follows.

DESCRIPTION OF APPARATUS

Wind tunnel.—The wind tunnel used in this investigation was the Langley 2- by 4-foot flutter research tunnel which is a single-return type equipped to use either air or Freon-12 as a test medium at pressures from 1 atmosphere down to about ⅛ atmosphere. The actual pressure and medium used will be discussed subsequently.

Airfoil and oscillator.—The airfoil used in determining the oscillatory normal forces and moments due to pitch had an NACA 65A010 airfoil section and a constant chord of 1 foot.

In addition to the tests of the clean airfoil, a few limited tests were performed with two different types of leading-edge disturbances and these are presented in appendix A. The model completely spanned the 2-foot dimension of the test section and was equipped with end plates which rotated with the airfoil to prevent tip leakage. The model was constructed from aluminum alloy that was machined in the form of two half shells with a solid section in the center to which were attached the pressure gages and the position indicator. The construction of the model is illustrated in figure 1.

The airfoil oscillator and general test configuration is illustrated in figure 2. Power to drive the wing is furnished by a synchronous-drive motor with a variable-frequency voltage supply. The speed of the drive motor, which was continuously controllable from 300 to 3,600 rpm, determined the frequency of oscillation. Attached to the motor shaft on both sides of the test section is the inner race of a bearing called an eccentric cam in figure 2. The eccentricity of this cam determines the amplitude of the oscillation. The oscillation is transmitted to the wing through a drive column

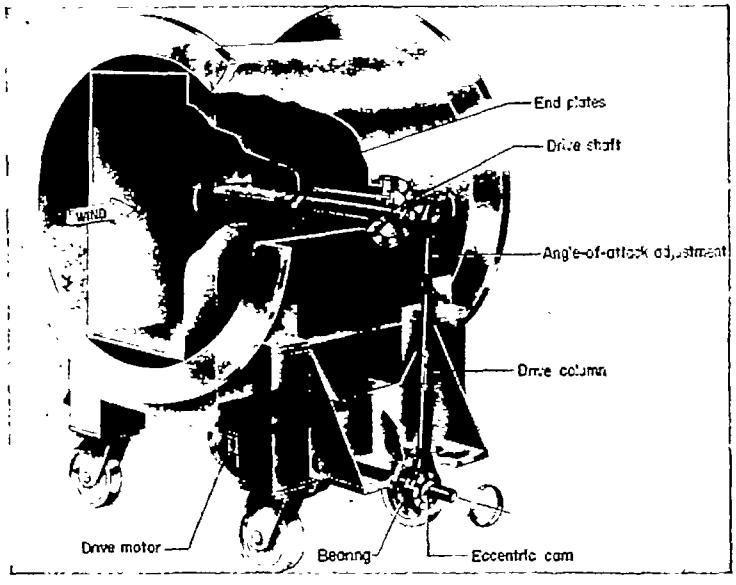

FIGURE 2.—Schematic drawing of model and oscillating mechanism.

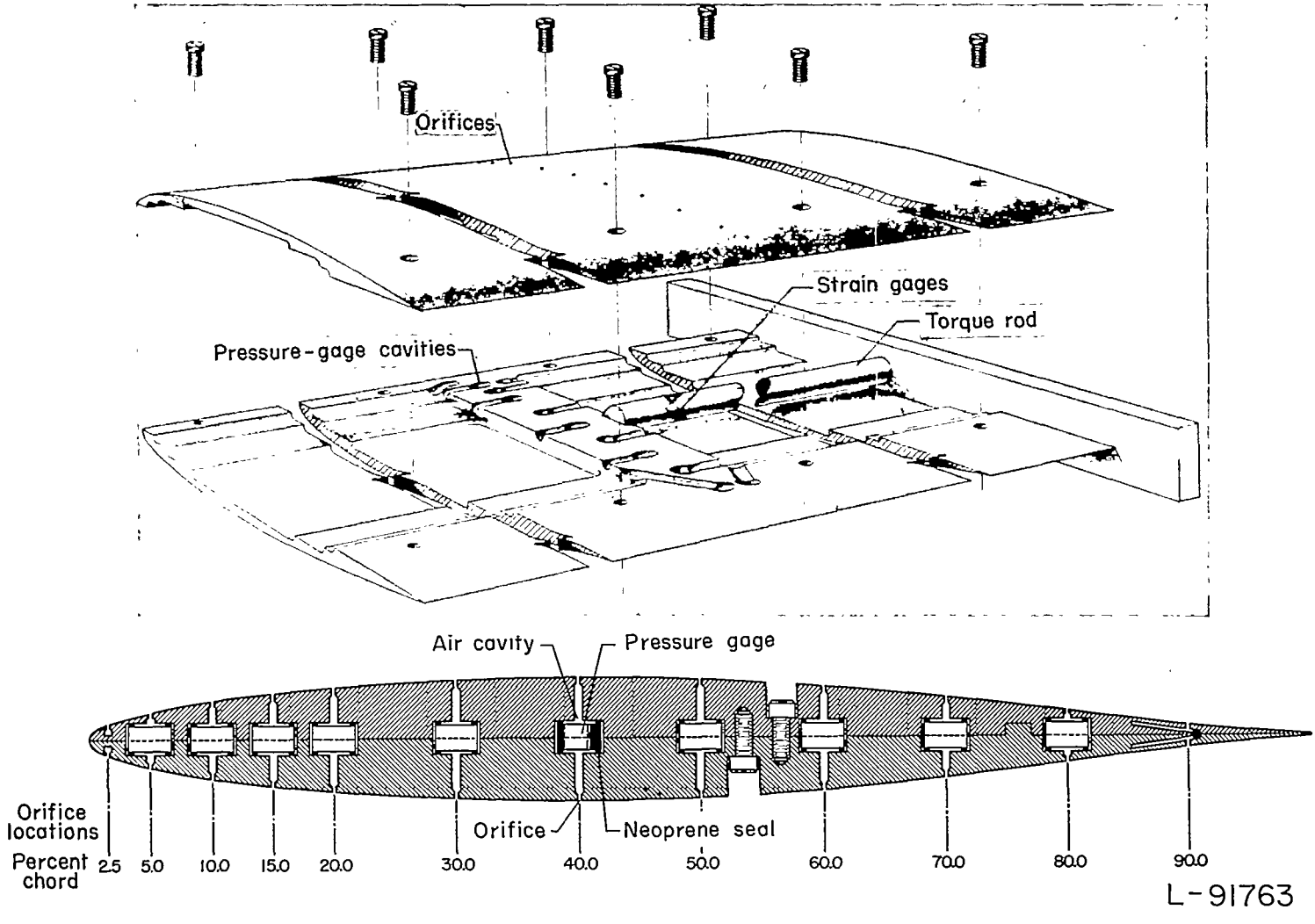

FIGURE 1.—Exploded view and cross section of model showing location of pressure gages, orifices, and position indicator.

(equipped with a turnbuckle for adjustment of mean angle of attack) pinned to a rocker arm which rotates a drive shaft attached to the airfoil.

Instrumentation.—The differential pressure acting on the wing was converted to an electrical signal by use of NACA miniature electrical pressure gages model 49–TP. (See ref. 10.) The 12 gages were located at 2.5, 5, 10, 15, 20, 30, 40, 50, 60, 70, 80, and 90 percent chord. The pressure-gage installation is illustrated in figure 1. The gages between 5 and 80 percent chord were clamped between the two wing halves and were connected to 0.030-inch-diameter orifices by 0.0625-inch-diameter drilled holes which had depths that varied with the thickness of the wing. The gages at 2.5 and 90 percent chord were connected to orifices by tubing which had an inside diameter of 0.040 inch and had lengths of 0.6 and 1.3 inches, respectively. The experimentally determined dynamic-response curves for the gages at 2.5, 90, and 20 percent chord are shown in figure 3. The resonant peaks occurring at high frequencies are associated with an acoustic phenomenon. The response curves presented in figure 3 were obtained at atmospheric pressure in air. The response characteristics of the pressure-gage-orifice installations have not been determined with Freon-12 as the ambient medium; however, it is believed that the systems have flat response to a sufficiently high frequency so that no response errors were involved in the measurements contained in this investigation which covers the frequency range from 0 to 35 cps.

The pressure-gage outputs were weighted and integrated electrically to give a signal proportional to lift or pitching moment. The weighting was computed on the basis that each gage represented the area or distance halfway between adjacent gages. For example, the first gage (at 2.5 percent c) was assumed to represent the area from the leading edge to the point halfway between the first gage and the second gage or an area of 3.75 percent of the total area. The second gage was assumed to represent the area or distance between 3.75 percent c and 7.5 percent c or an area of 3.75 percent of the total area. For pitching moments, each area was multiplied by the distance from its centroid to the reference axis. The principles and details of electrical integration are discussed in reference 11.

The angular motion of the center-line station of the airfoil was converted to an electrical signal by means of a torsion rod which is illustrated in figure 1. A resistance-wire-strain-gage bridge arranged to indicate torsional strains was attached to a steel rod 0.5 inch in diameter which had one

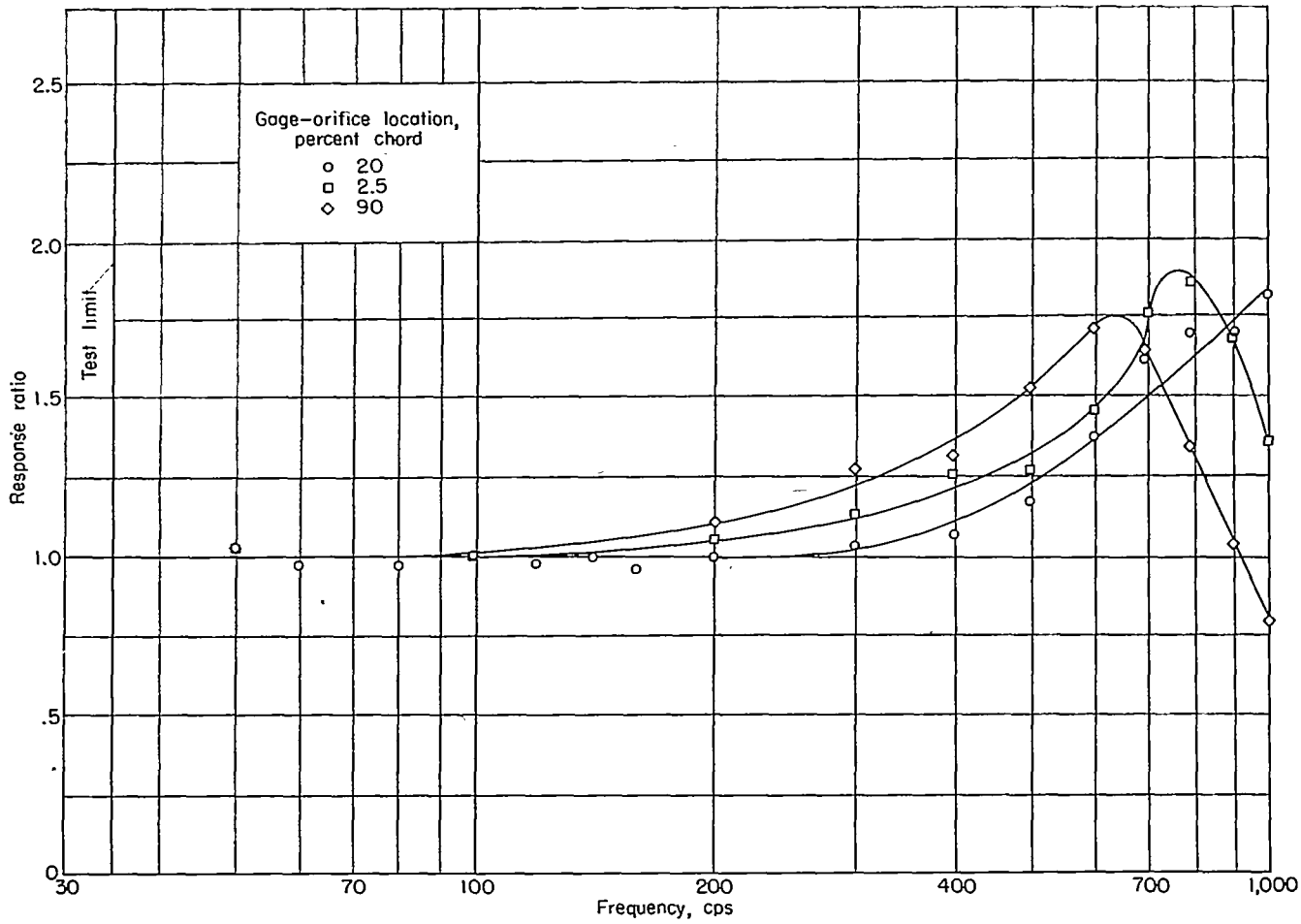

FIGURE 3.—Dynamic response characteristics of three pressure-gage-orifice installations.

end fixed to the center of the airfoil and the other end fixed to the tunnel wall. The first natural frequency of the rod in torsion was estimated to be about 700 cps.

A block diagram of the instrumentation is shown in figure 4. The electrical signals proportional to normal force or pitching moment and angular displacement were operated on in a variety of ways by suitable switching arrangements.

Time-history records of the lift or pitching moment and angular displacement were obtained by use of a recording oscillograph. Some observations on the time histories of individual pressures on an oscillating airfoil near the stall are presented in appendix B.

The magnitude of the fundamental normal-force or pitching-moment vector was determined by feeding the signal through a narrow band-pass variable-frequency filter which was tuned to the frequency of oscillation. The signal out of the filter was then amplified through a linear amplifier and fed into a vacuum thermocouple, the output of which was read on a heavily damped microammeter. This heavily damped mean-square indicating device was required because of the fluctuations in normal force or pitching moment encountered at the high-angle-of-attack conditions.

The phase angle of the fundamental component of the normal force or pitching moment with respect to the angular displacement was obtained by passing both the normal-force or moment and angular-displacement signals through identical channels of the narrow band-pass filter then into identical channels of a pulse-shaping device. The pulse shaper consisted, essentially, of several stages of amplification, clipping, and differentiation which resulted in conversion of the input sine wave to a series of sharp pulses corresponding in time to the positive crossover points of the sine wave. The phase angle between normal force and position was then obtained by starting an electronic chronograph with the leading signal and stopping the chronograph with the lagging signal. The time obtained in this manner was the time lag between normal force or moment and position which, when divided by the period of the oscillation and multiplied by 360°, yielded the phase angle in degrees. A similar method of measuring phase angles, which was developed independently, is described in detail in reference 12. The period of the oscillation was obtained by starting and stopping the chronograph with a single signal, usually the angular displacement. Of course, slight differences in components and tuning caused extraneous shifts in phase between the two signals. This tare phase angle was measured during each measurement of phase angle by feeding a single signal (usually the angular displacement) through both channels.

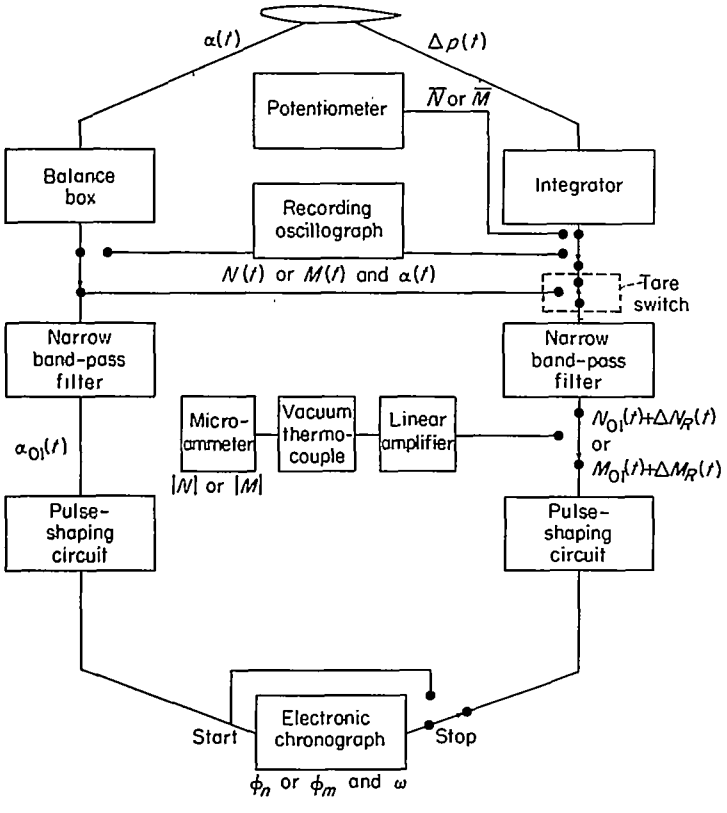

FIGURE 4.—Block diagram of instrumentation used for two-dimensional tests.

PROCEDURE

The aerodynamic normal forces and pitching moments acting on the two-dimensional airfoil oscillating in pitch were determined at Mach numbers of 0.35 and 0.7 and at a Reynolds number of 5.3×10^6. Freon–12 was used as a test medium. The Reynolds number was held constant by reducing the tunnel pressure from 1 atmosphere for the tests at a Mach number of 0.35 to about ½ atmosphere for the tests at a Mach number of 0.7.

After the desired tunnel velocity and pressure had been obtained, the mean angle of attack was adjusted by use of the turnbuckles shown in figure 2. The zero-frequency increment in normal force or moment was then obtained with the model set at its two extremes; this setting was accomplished by turning the oscillator shaft through one complete revolution very slowly. The incremental voltage corresponding to the incremental force or moment was obtained from a self-balancing potentiometer.

After the zero-frequency measurements were made, the drive motor was started and brought to a speed corresponding to an airfoil oscillation frequency of approximately 10 cps. The lower limit of frequency was determined by the low-frequency limit of the narrow band-pass variable-frequency filter. After the desired frequency had been reached, the normal-force or pitching-moment and position signals were operated on in the manner previously described to obtain the quantities of interest. The frequency was then increased in increments of about 5 cps to a maximum frequency of about 35 cps. Data were not obtained at frequencies above 35 cps because of the uncertainties of the effect of wind-tunnel walls as indicated in reference 9.

This procedure was repeated at initial angles of attack of 0°, 4°, 8°, 12°, and 16° at a Mach number of 0.35; also 0°, 4°, 6°, and 8° at a Mach number of 0.7. The amplitude of oscillation for all conditions was about 1.2°.

DATA REDUCTION

The forces acting on an oscillating wing under separated-flow conditions may be thought of as being composed of three parts: (1) the steady or mean component, (2) those forces which are related in time to the motion, that is, have a definite phase relationship, and (3) those forces which are not correlated with the motion. The third type of unsteady forces will be random in character and probably will be similar, at least, to the fluctuating forces which act on a stationary rigid wing when it is stalled. At low angles of attack, a random force existed which was small (about twice the instrument noise level) and, presumably, was due to residual tunnel turbulence. At high angles of attack, the random forces were of the order of ten times the random forces which existed at low angles of attack; and, consequently, consideration had to be given to ways and means of accounting for these forces in making the desired measurements.

This composition of forces may be expressed simply as follows:

$$N(t)=\overline{N}+N_0(t)+N_R(t)$$

where $\overline{N}$ denotes the steady-state force associated with the mean angle of attack $\bar{\alpha}$, $N_0(t)$ refers to the oscillating forces which are related to the sinusoidal motion $\alpha(t)=|\alpha|e^{i\omega t}$, and $N_R(t)$ designates the random forces which are not correlated with the motion. The problem, then, is to separate properly the three types of forces so that the significant properties can be determined. This separation can be done in several ways. The method used in these tests of the two-dimensional model consisted of passing the normal-force or pitching-moment signal through a narrow band-pass variable-frequency filter tuned to the frequency of oscillation. In this manner, a large part of the random forces, as well as the mean force, were rejected; therefore, only the fundamental force or moment vector and the random parts lying within the band pass of the filter were left. The possible existence and importance of higher harmonics in the force or moment is discussed in appendix C.

The output of the filter is illustrated vectorially in figure 5. The large vector representing the fundamental component of normal force or pitching moment is fixed in phase, but the small vector representing the random part of the force or moment not rejected by the filter rotates randomly about the end of the fundamental component and varies randomly in length. The resultant vector will vary randomly in both magnitude and phase over a small range. Since the phase-measuring technique yielded the phase angle for a single cycle of oscillation, it was necessary to obtain several values for a given condition. The arithmetic mean of the several values was used as the best value to represent the phase of the fundamental component. The number of values taken at each test condition was increased or decreased according to the range of fluctuation encountered. Usually about 10 values were considered sufficient.

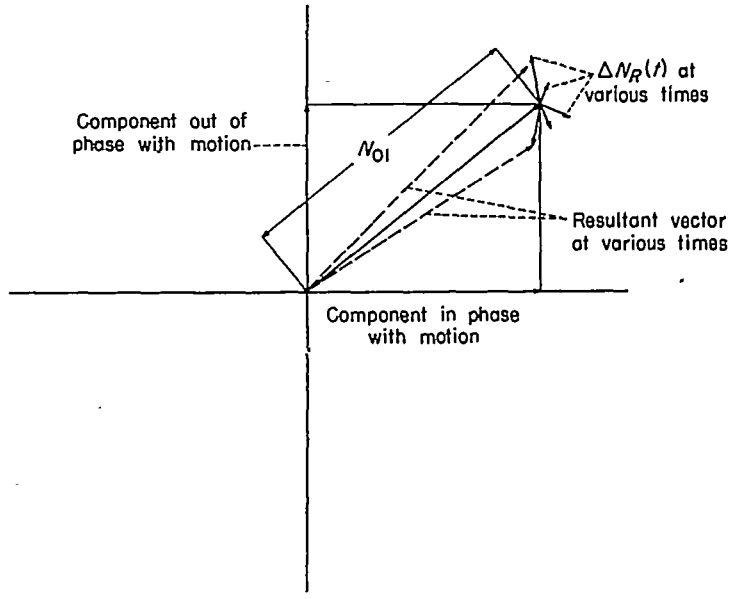

FIGURE 5.—Vector diagram of filter output tuned to frequency of oscillation.

The magnitude of the fundamental component of normal force or pitching moment was obtained by passing the output of the filter through a mean-square indicating device which performed the following operation:

$$\frac{1}{2T}\int_{-T}^{T}[N_{01}(t)+\Delta N_R(t)]^2dt=\overline{N_{01}^2}+2\overline{N_{01}\Delta N_R}+\overline{\Delta N_R^2}$$

where N_{01} is the fundamental component, ΔN_R is the part of the random force lying within the band pass of the filter, and T is an arbitrary period of time. Since the time average of the product of two uncorrelated quantities must be zero, the reading of the mean-square meter will be proportional to $\overline{N_{01}^2}+\overline{\Delta N_R^2}$. The value of $\overline{N_{01}^2}$ was obtained by subtracting the meter reading with the airfoil held rigid at the mean angle of attack from the meter reading during the oscillation.

This operation assumes that the random forces are not affected by the oscillation. The severity of this assumption involves at least two conditions. Since the intensity of the random forces is a function of angle of attack, a modulation of the random forces at the frequency of the variation in angle of attack might be expected. This effect has been minimized by obtaining the estimates of $\overline{\Delta N_R^2}$ at the mean angle of attack.

An additional effect of the oscillation on the random forces might result from a change in the general character of the separated flow from the stationary case to the oscillating case. For example, the oscillation of the airfoil might alter

the boundary-layer stability in such a way as to cause a change in both the intensity and frequency content of the fluctuating forces. The possibility of a flow change of this type is a difficult one to check; however, some information supporting the validity of the assumption used in obtaining $\overline{N_{01}^2}$ from the meter readings has been obtained. With the airfoil held stationary at the mean angle of attack; an estimate of the frequency content of the random forces was obtained by tuning the narrow band-pass filter to various frequencies within the range of interest. Similar measurements were made with the airfoil oscillating at a particular frequency about the mean angle of attack. The frequency content for these two conditions are compared with the filter characteristic function in figure 6. The data for the condition where the wing was held stationary indicate a relatively smooth, low level of fluctuating forces. The data obtained with the wing oscillating are similar to that for the stationary wing except in the vicinity of the oscillation frequency. Near the wing oscillation frequency, the curve representing the filter characteristic function would be a good fairing of the data obtained with the wing oscillating; and, since the filter characteristic curve represents the filter output to a single frequency input, it can be concluded that the primary effect of oscillating the airfoil on the frequency content of the air forces was the addition of a single component at the frequency of oscillation.

In addition to the aerodynamic normal force, the vector N_0 contains a small component due to the inertia effects on the pressure gages. The magnitude of this tare-acceleration effect was determined by oscillating the airfoil in a near vacuum and is shown in figure 7. These tare values were subtracted vectorially from the N_{01} determinations. The

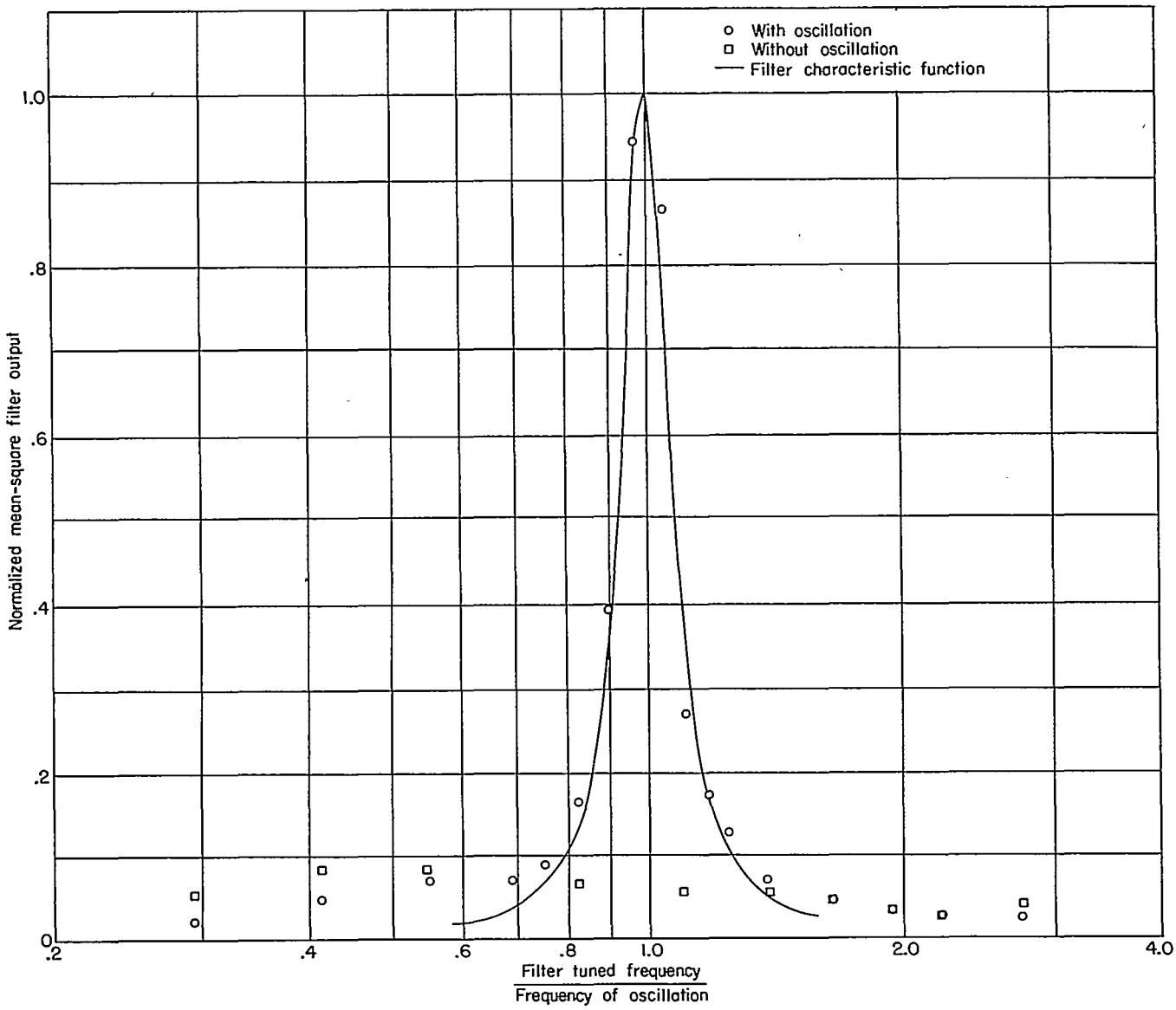

FIGURE 6.—Comparison of normal-force filter output with and without oscillation with filter characteristic function. $\alpha=12°$; $f=35$ cps; and Mach number of 0.35.

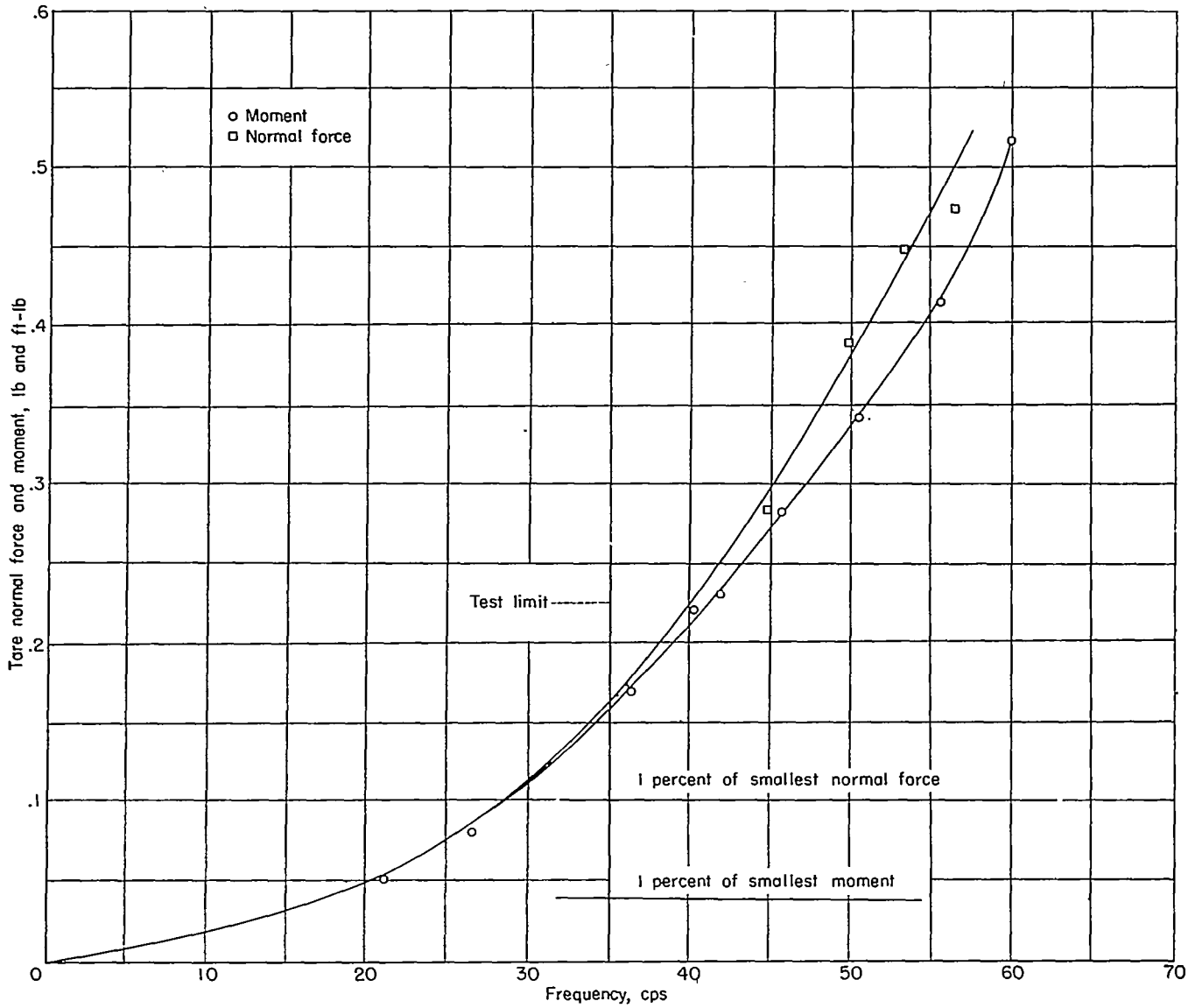

FIGURE 7.—Apparent normal force and pitching moment due to inertia of pressure-gage diaphragm.

tare values were kept small relative to the aerodynamic components by conducting the tests at as high a value of dynamic pressure as was consistent with the required Mach number and Reynolds number. Lines representing 1 percent of the smallest oscillating normal force and pitching moment are indicated in figure 7. The tare value in the worst case amounted to about 4 percent of the magnitude of the fundamental component of pitching moment and caused a phase correction of about 2°.

Because of the inertia and flexibility of the mechanical system, the absolute magnitude of the pitching oscillation was a function of frequency even though the motion of the positive-displacement drive mechanism remained at the design value of $|\alpha|=1.2°$. It was found that the airfoil itself did not distort appreciably along its span, but there was a sizeable twisting of the drive shafts relative to the rocker arms outside the test section. Tests indicated that this twisting or distortion of the system was not affected by air forces; consequently, it was possible to use a single function to represent the variation of the absolute magnitude of the pitching oscillation with frequency. This function is shown in figure 8.

After the absolute magnitudes of the fundamental components of aerodynamic normal force and pitching moment had been determined from the meter readings by use of suitable calibration constants, they were converted into coefficient form according to the following definitions:

$$\left|\frac{dc_n}{d\alpha}\right|=\frac{|N|}{\frac{1}{2}\rho V^2 S|\alpha|}$$

and

$$\left|\frac{c_m}{d\alpha}\right|=\frac{|M|}{\frac{1}{2}\rho V^2 Sc|\alpha|}$$

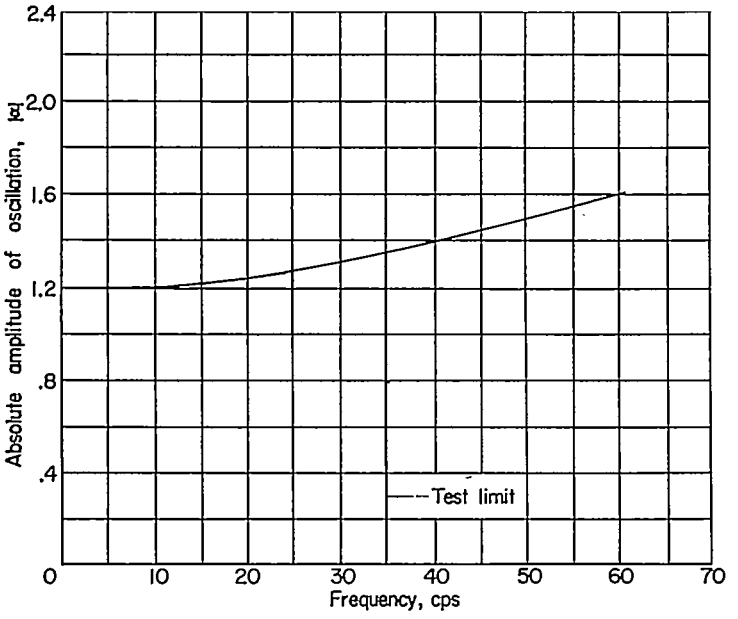

FIGURE 8.—Variation with frequency of absolute amplitude of oscillation of two-dimensional airfoil.

where $|\alpha|$ is measured in radians.

The sign convention used in orienting the vector defines upward normal force, nose-up pitching moment, and nose-up pitch deflection as positive.

The component of pitching-moment coefficient which is in phase with the angular velocity is related to the damping; therefore, the damping coefficient is defined as $\left|\frac{dc_m}{d\alpha}\right| \sin \phi_m$. The sign convention used in describing the coefficients of damping in pitch is illustrated in the following vector diagram:

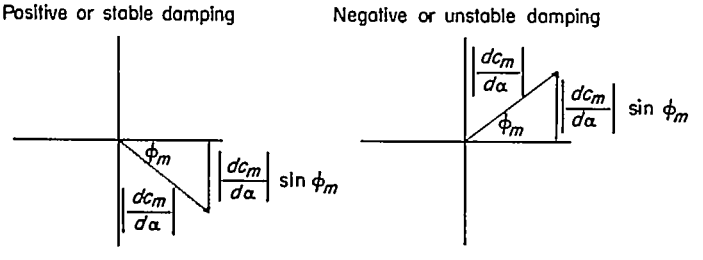

RESULTS AND DISCUSSION

The magnitude and phase of the fundamental components of oscillatory normal-force and pitching-moment coefficients for the two-dimensional NACA 65A010 airfoil oscillating in pitch about the midchord are shown in figures 9 to 12 as functions of reduced frequency for various angles of attack. The coefficients of damping in pitch $\left|\frac{dc_m}{d\alpha}\right| \sin \phi_m$ are shown as functions of reduced frequency in figures 13 and 14.

LOW ANGLES OF ATTACK

For purposes of comparison, the theoretical normal forces and pitching moments calculated for compressible, two-dimensional flow are shown along with the measured two-dimensional data in figures 9 to 12. The theoretical coefficients used are those which are presented in reference 13 and which are modified to agree with the sign convention and coefficient form used in this report.

Examination of figures 9 and 10 indicates that the forces and moments measured at $\bar{\alpha}=0°$ and $\bar{\alpha}=4°$ compare very well with the theoretical values at a Mach number of 0.35. The conventional steady-state section normal-force and section pitching-moment coefficients have been measured for a Mach number of 0.35 and a Reynolds number of 5.3×10^6 and are presented as functions of angle of attack in figure 15. These data indicate a linear relation between both normal-force and pitching-moment coefficients and angle of attack up to an angle of attack of about 7°. Tuft studies conducted at these same conditions indicated no disturbances on the upper surface until an angle of attack of 6° was reached. With the airfoil in a clean condition (that is, with no tufts attached), oscillographic observation of the outputs of the individual pressure gages indicated no pressure fluctuations up to an angle of attack of 7.6°. It appears reasonable, then, that there were no important boundary-layer effects on the static normal forces and pitching moments for angles of attack up to at least 6°. Furthermore, the oscillatory derivatives are not expected to vary appreciably with the mean angle of attack so long as the airfoil remains in the unseparated-flow condition throughout the range of oscillation.

Examination of figures 11 and 12 indicates that, at a Mach number of 0.7, the data for both $\bar{\alpha}=0°$ and $\bar{\alpha}=4°$ differ appreciably from theory. The discrepancy between theory and experiment at $\bar{\alpha}=0°$ may be attributed primarily to effect of wind-tunnel walls. No corrections have been applied to the data to account for the presence of the walls. Both the theory and experiments of reference 9 indicate an increase in the effect of tunnel walls when the Mach number is increased from 0.35 to 0.7. (Ref. 9 gives a comparison between theory and experiments on the same two-dimensional model as that used in the present investigation. This comparison shows good agreement between the measured forces and moments and those calculated which included the effect of the walls.)

The discrepancies between the data for $\bar{\alpha}=4°$ and the theory may be due, in part, to tunnel-wall effects or to boundary-layer and shock effects. There is virtually no information available concerning the effect of angle of attack on the wind-tunnel-wall corrections for oscillating air forces; however, it appears reasonable that the effects of the walls might be greater at higher angles of attack because of the increased blockage. The static normal-force and pitching-moment coefficients measured at a Mach number of 0.7 are shown in figure 16. Examination of these static coefficients indicates a degree of nonlinearity in both the normal-force and pitching-moment curves which may be due to the possible causes mentioned previously.

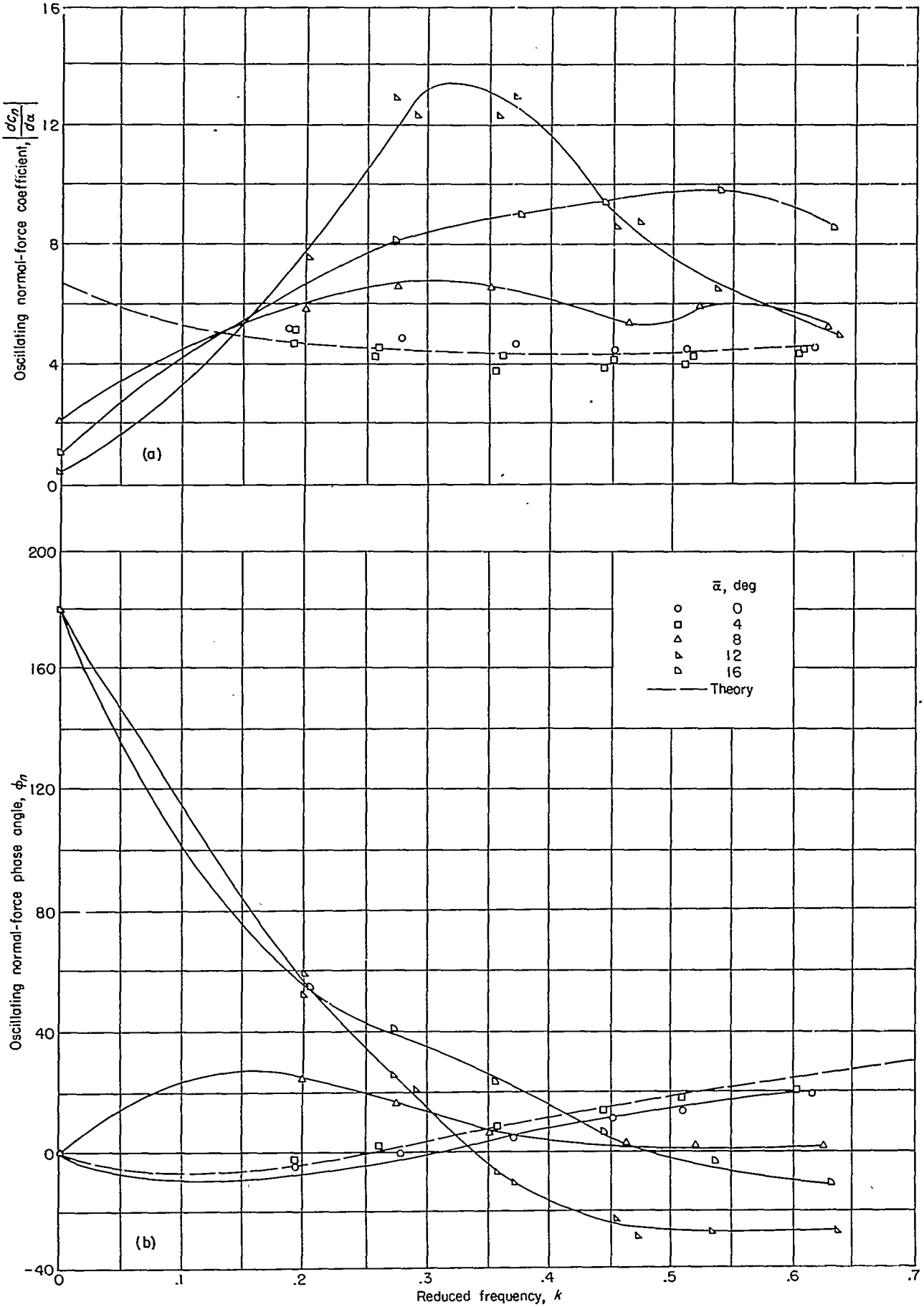

(a) Magnitude.
(b) Phase angle.

FIGURE 9.—Variation of normal-force coefficient with reduced frequency for two-dimensional 65A010 airfoil oscillating in pitch about the midchord at Mach number of 0.35.

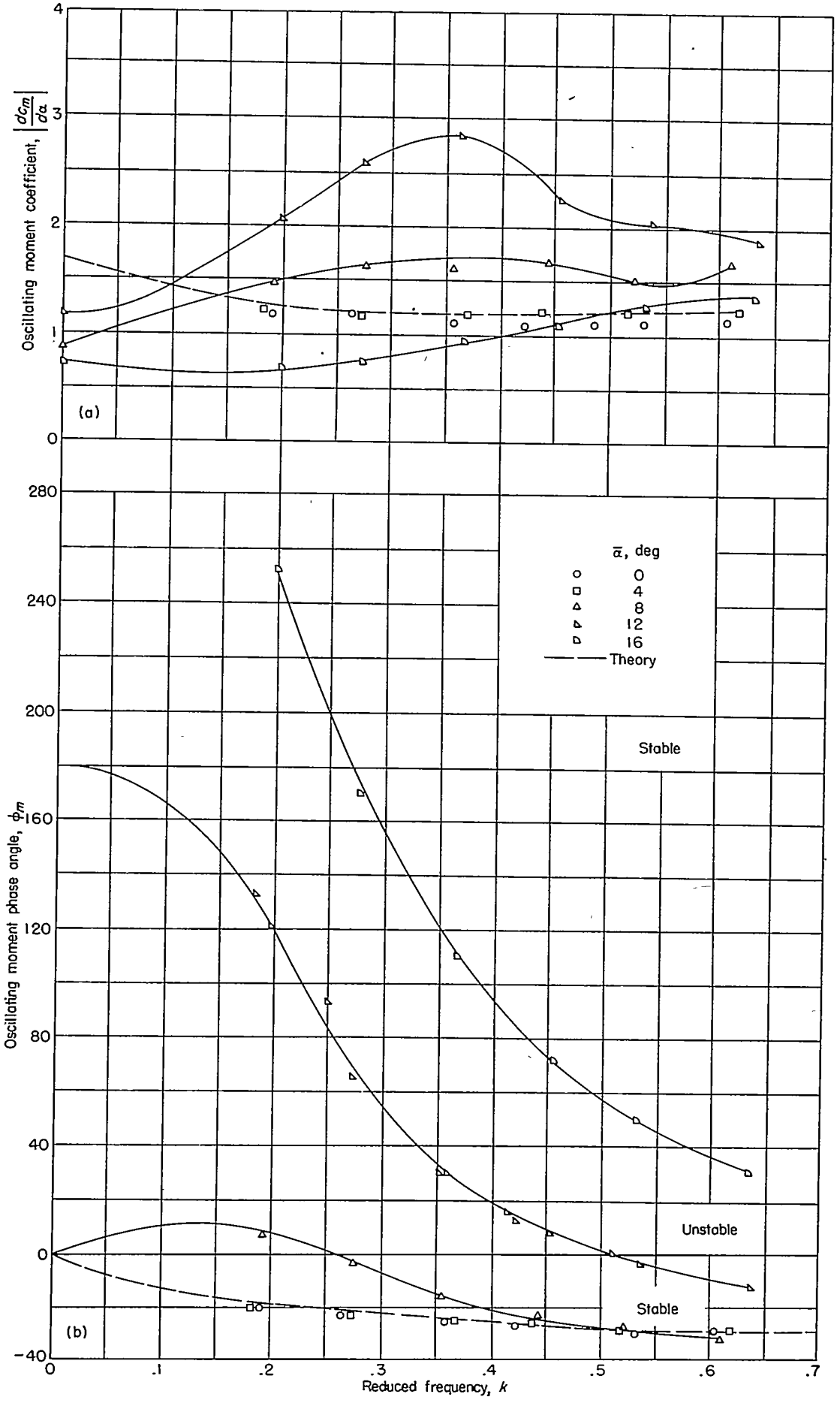

(a) Magnitude.
(b) Phase angle.

FIGURE 10.—Variation of pitching-moment coefficient with reduced frequency for two-dimensional 65A010 airfoil oscillating in pitch about the midchord at Mach number of 0.35.

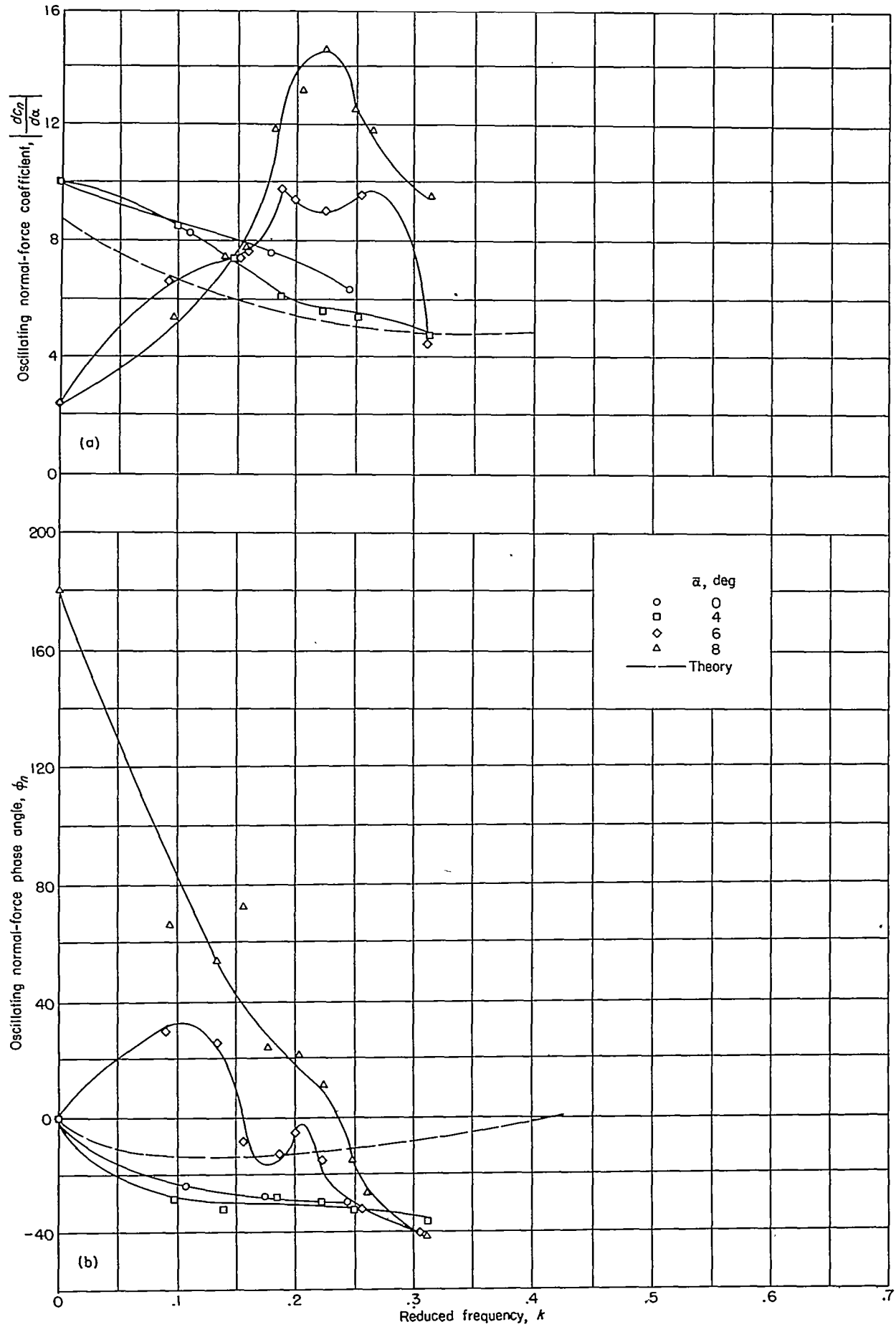

(a) Magnitude.
(b) Phase angle.

FIGURE 11.—Variation of normal-force coefficient with reduced frequency for two-dimensional 65A010 airfoil oscillating in pitch about the midchord at Mach number of 0.7.

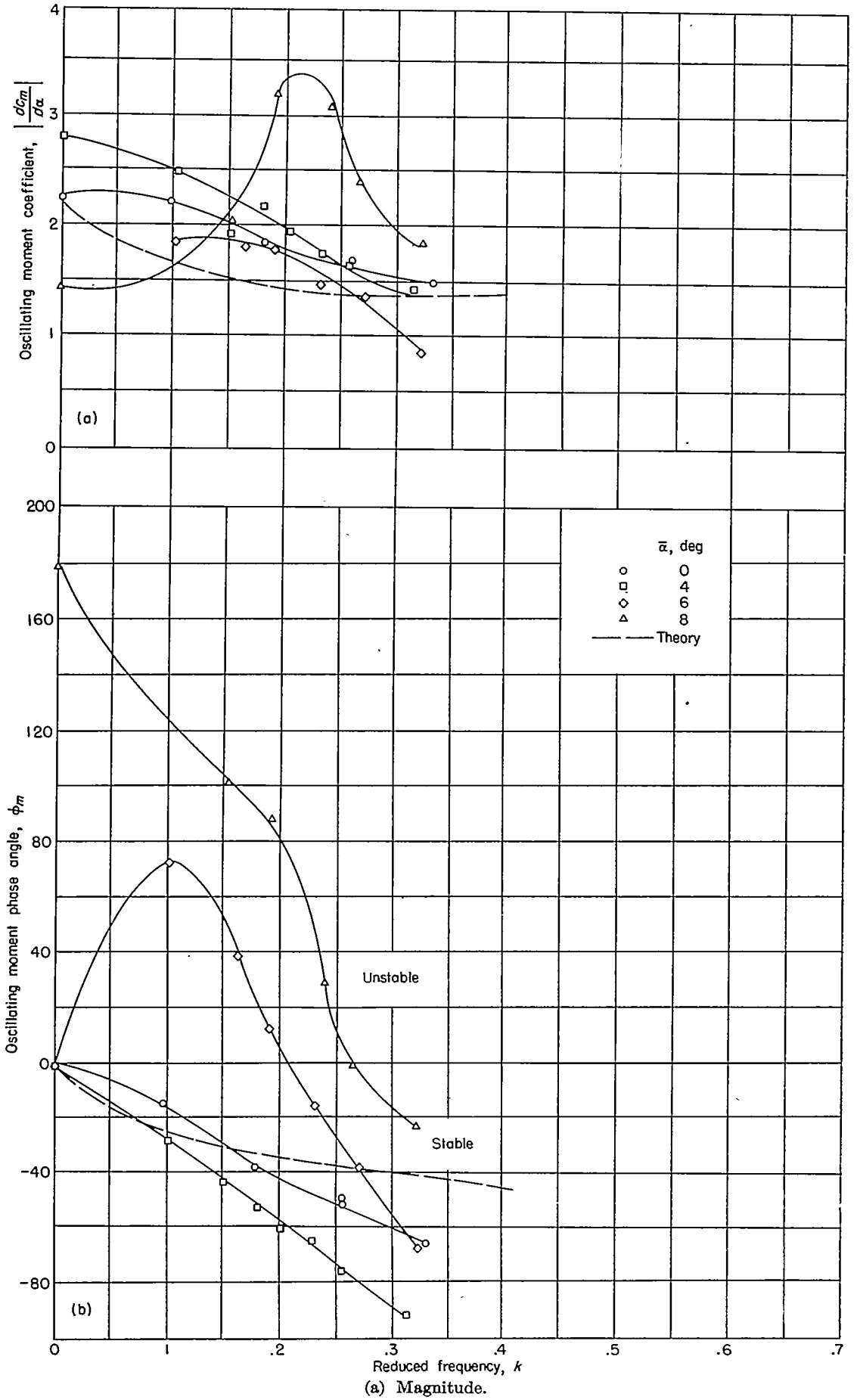

(a) Magnitude.
(b) Phase angle.

FIGURE 12.—Variation of pitching-moment coefficient with reduced frequency for two-dimensional 65A010 airfoil oscillating in pitch about the midchord at Mach number of 0.7.

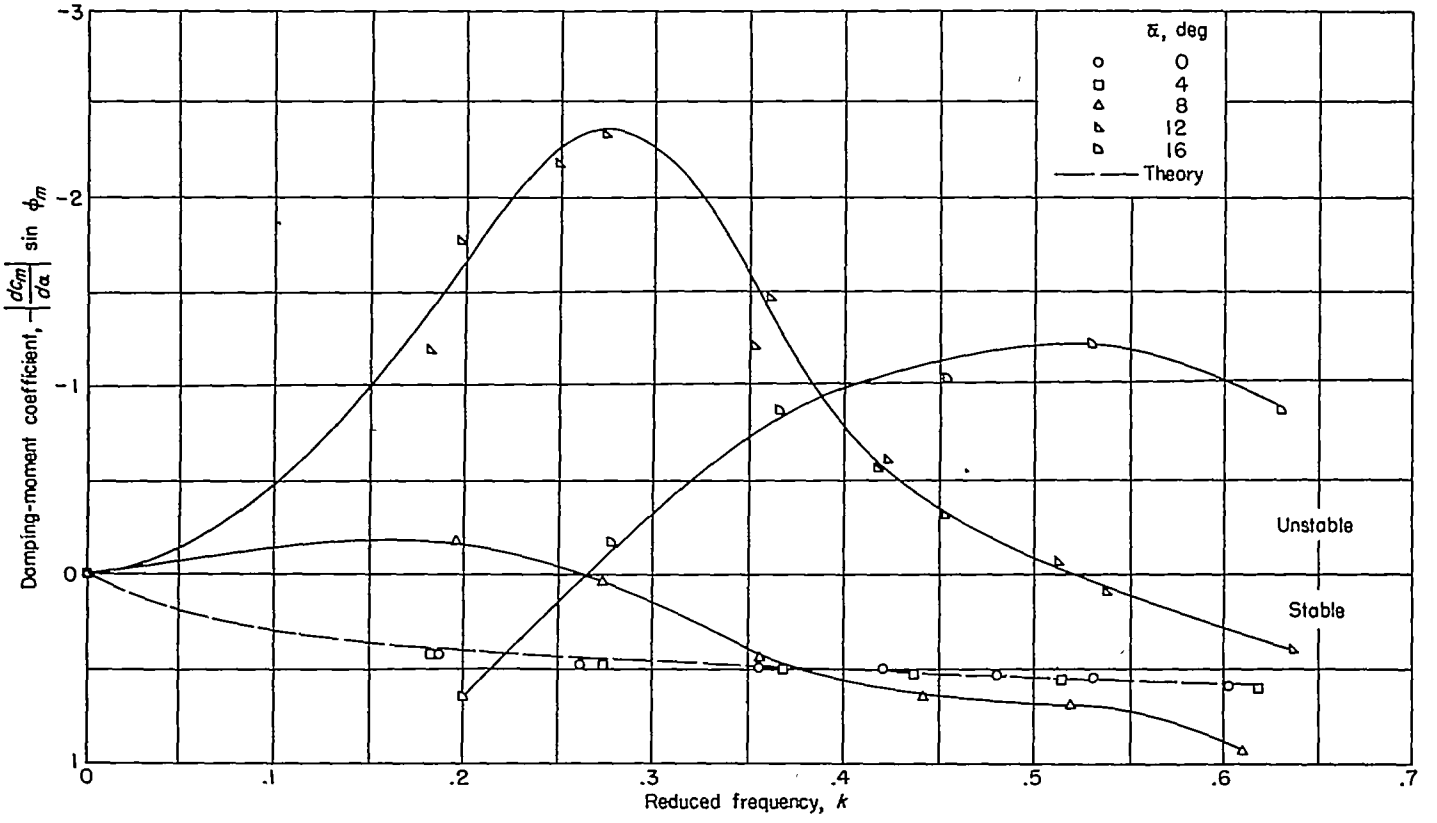

FIGURE 13.—Variation of damping-moment coefficient with reduced frequency for two-dimensional 65A010 airfoil oscillating in pitch about the midchord at Mach number of 0.35.

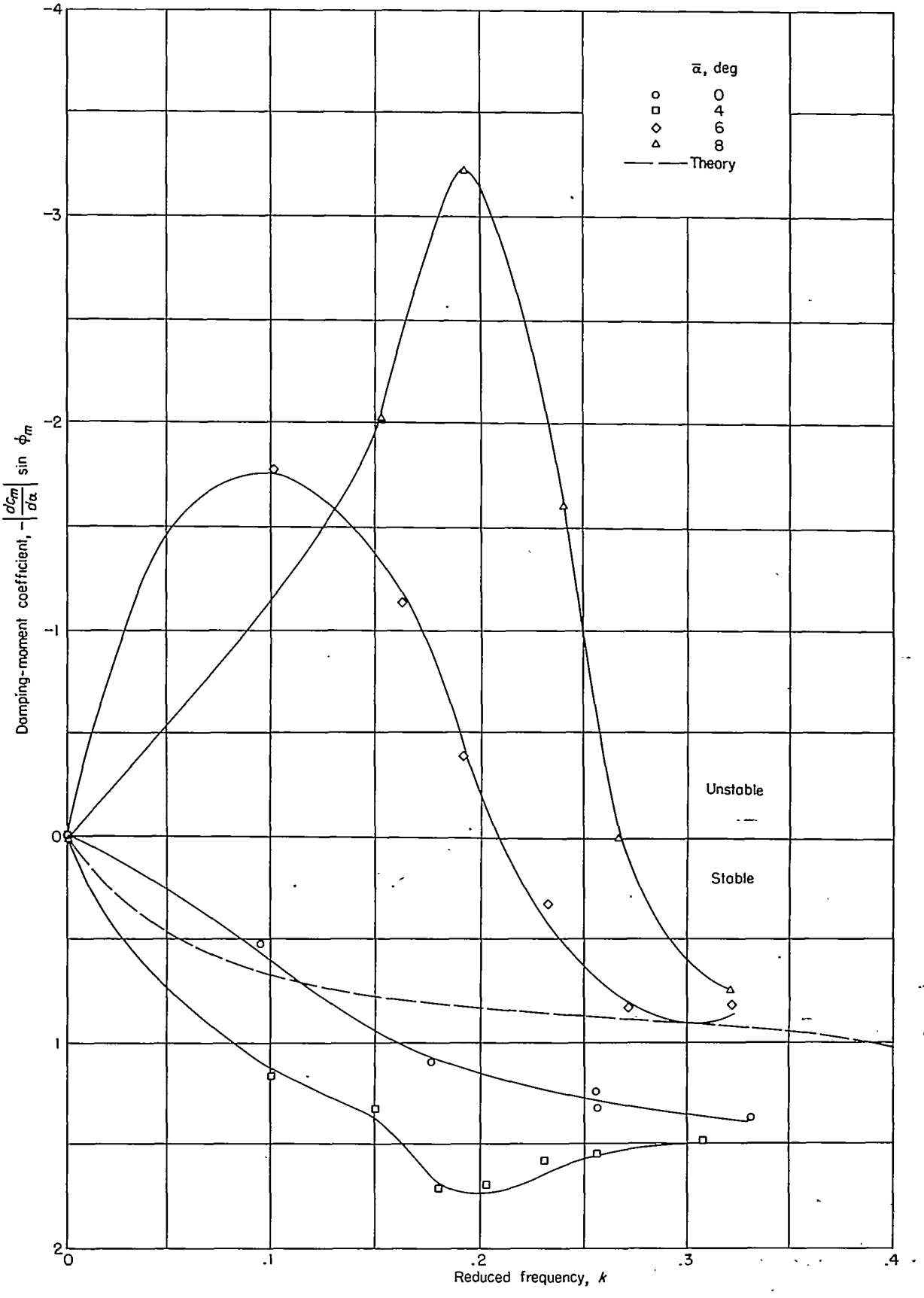

FIGURE 14.—Variation of damping-moment coefficient with reduced frequency for two-dimensional 65A010 airfoil oscillating in pitch about the midchord at Mach number of 0.7.

460194—58——35

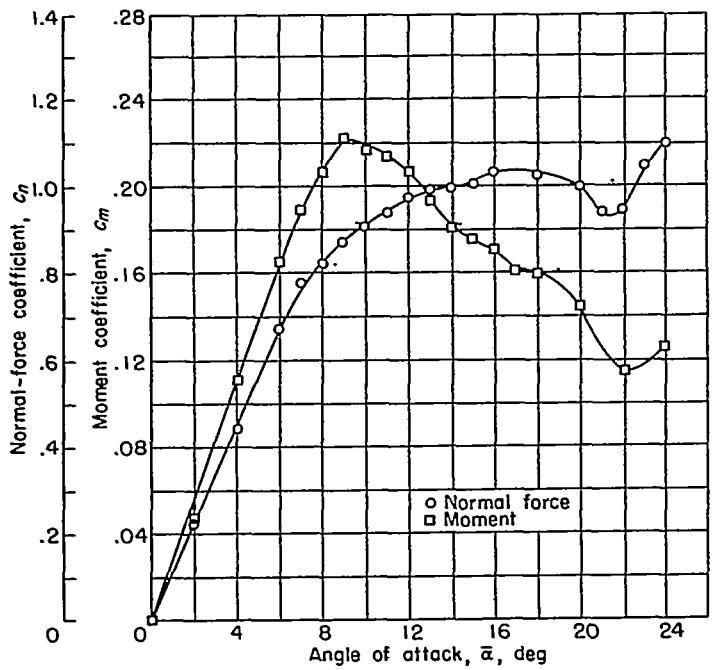

FIGURE 15.—Variation of static-normal-force and static-pitching-moment coefficients with angle of attack for two-dimensional 65A010 airfoil at Mach number of 0.35.

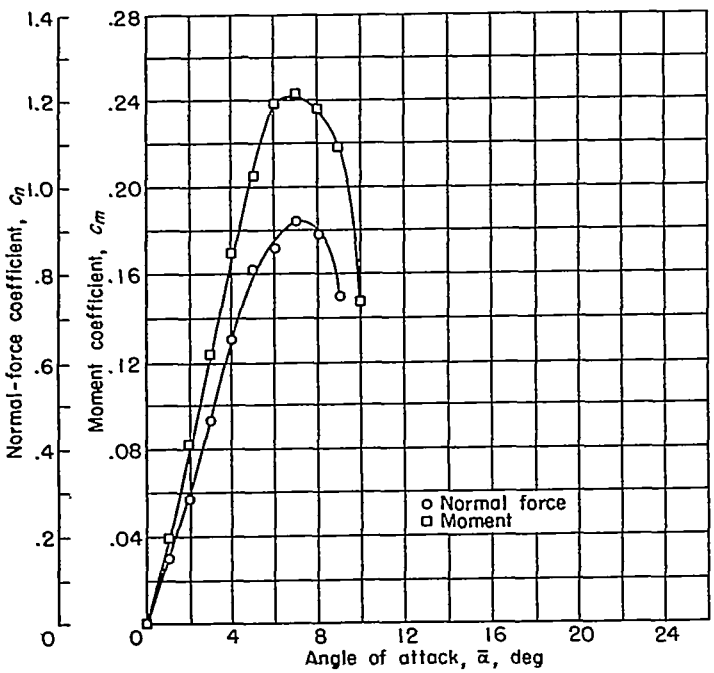

FIGURE 16.—Variation of static-normal-force and static-pitching-moment coefficients with angle of attack for two-dimensional 65A010 airfoil at Mach number of 0.7.

HIGH ANGLES OF ATTACK

The normal-force and pitching-moment coefficients measured at angles of attack higher than $\bar{\alpha}=4°$ (figs. 9 to 12) differ appreciably from the coefficients measured at lower angles of attack. At zero frequency and high mean angles of attack, the magnitude of the change in normal force or pitching moment with change in angle of attack is considerably reduced from that obtained at small mean angles. In addition, in some cases the sign of the change in force or moment is reversed as indicated by values of the phase angle occurring at 180°. At frequencies other than zero, however, the magnitude of the forces and moments in some cases are much higher than those observed at low angles.

Inasmuch as the coefficients of normal force and pitching moment presented in figures 9 to 12 correspond to slope of the lift curve or moment curve, it may appear somewhat surprising to observe much higher values for angles of attack near the stall than occurred at small angles of attack. This result has been obtained before. (See refs. 14 and 15, for example.) Although the mechanism of this phenomena has not been established, a few speculative remarks may be made. If it is reasoned that the airfoil with separated flow may be replaced by a new airfoil having dimensional characteristics determined by the boundary layer, it does not appear inconceivable that this imaginary airfoil could, under some oscillating conditions, undergo large changes in camber during the oscillation which, in turn, could produce much larger changes in normal force and pitching moment than would be expected of a nondeforming airfoil. Jones (ref. 4) has incorporated this feature of a variable-camber airfoil with some success in an attempt to calculate oscillating air forces at high angles of attack. However, the establishment of the time behavior of this imaginary airfoil would be a complicated problem.

In addition to the large effects of increased angle of attack on the magnitudes of normal force and pitching moment, there were also large effects on the phase angles. The effect of angle of attack on the moment phase angles is such that under some conditions the aerodynamic-damping moment is unstable. This result is illustrated in figures 13 and 14 where the imaginary or damping component of the pitching-moment coefficient has been plotted as a function of reduced frequency. The existence of regions of unstable damping implies the possibility of single-degree-of-freedom flutter in the torsion mode.

Examination of figures 13 and 14 indicates that the effect of increasing the Mach number from 0.35 to 0.7 was primarily to decrease the initial mean angle of attack at which unstable damping moments occurred. This result, presumably, was due to larger adverse pressure gradients which caused boundary-layer effects.

The existence of the large regions of angle of attack and reduced frequency at which unstable damping in pitch occurs is in direct contrast to the measurements of damping in the bending mode of finite-span wings which will be discussed subsequently.

FINITE-SPAN WINGS OSCILLATING IN FIRST BENDING MODE

TECHNIQUE

The aerodynamic damping for finite-span wings oscillating in the first bending mode was measured by use of a technique based on measurements of the power required to maintain oscillation at the natural frequency of the system. In order to eliminate from the measurements the presence of

relatively large random forces which acted on the wings at high angles of attack, a wattmeter was used as an indicator of the power required to maintain oscillation. It may be recalled that a wattmeter is a phase-sensitive device; and, since the phase of the random forces relative to the position of the wing is just as likely to cause a momentary increase in the power reading as it is to cause a momentary decrease, there will be no net effect of the random forces on the average reading of the wattmeter. A more detailed description of the technique follows.

DESCRIPTION OF APPARATUS

Wind tunnel.—The Langley 2- by 4-foot flutter research tunnel, described previously, was also used for the tests of the finite-span models.

Models and oscillator.—The two semispan models used for the bending measurements differed primarily in airfoil thickness. The 10-percent-thick wing was rectangular in plan form and had NACA 65A010 airfoil sections. The wing had a chord of 8 inches, a semispan of 20 inches, and thus an aspect ratio of 5.0. The strength and stiffness of the 10-percent wing were concentrated in an aluminum-alloy core $\frac{5}{32}$ inch thick, the airfoil being filled out by balsa glued to the core with the grain oriented vertically to the plane of the wing. The 3-percent-thick wing was tapered in plan form and had NACA 16–003 airfoil sections. This wing had a root chord of 10 inches, a tip chord of 5 inches, and thus a taper ratio of 0.5. The semispan of 16 inches resulted in an aspect ratio of 4.27. The 3-percent wing was constructed of solid aluminum alloy. Both the 10-percent wing and the 3-percent wing had zero sweep of the midchord axis.

The finite-span models were clamped at the root and oscillated in, essentially, the first bending mode by a wire attached to the wing and to an electromagnetic shaker as shown schematically in figure 17. Since it was necessary to maintain a net tension in the wire between the shaker and the wing, in order for the shaker to apply a sinusoidal force to the wing, an external cantilever spring was installed between the shaker and the wing. The net effect of the additional stiffness and mass of the external wire-spring-shaker-coil system was to increase the first natural frequency of the 10-percent wing from 11.3 cps to 26 cps. The increase for the 3-percent wing was from 43 cps to 50 cps. The effect of the additional stiffness and mass on the oscillatory deflection modes for the two wings is illustrated in figure 18, where the shapes of the fundamental bending mode calculated for the wings as simple cantilevers are compared with the measured mode shapes of the wings oscillating at the first natural frequency of the combined system. The deflection modes were measured by use of a time-exposure photographic technique. (See ref. 16.)

Instrumentation.—Both the 10-percent wing and the 3-percent wing were equipped with resistance-wire-strain-gage bridges arranged to indicate strains in bending and torsion. The bending gages were used as a qualitative measure of amplitude of oscillation.

A block diagram of the instrumentation used in conjunction with the electromagnetic shaker is shown in figure 19.

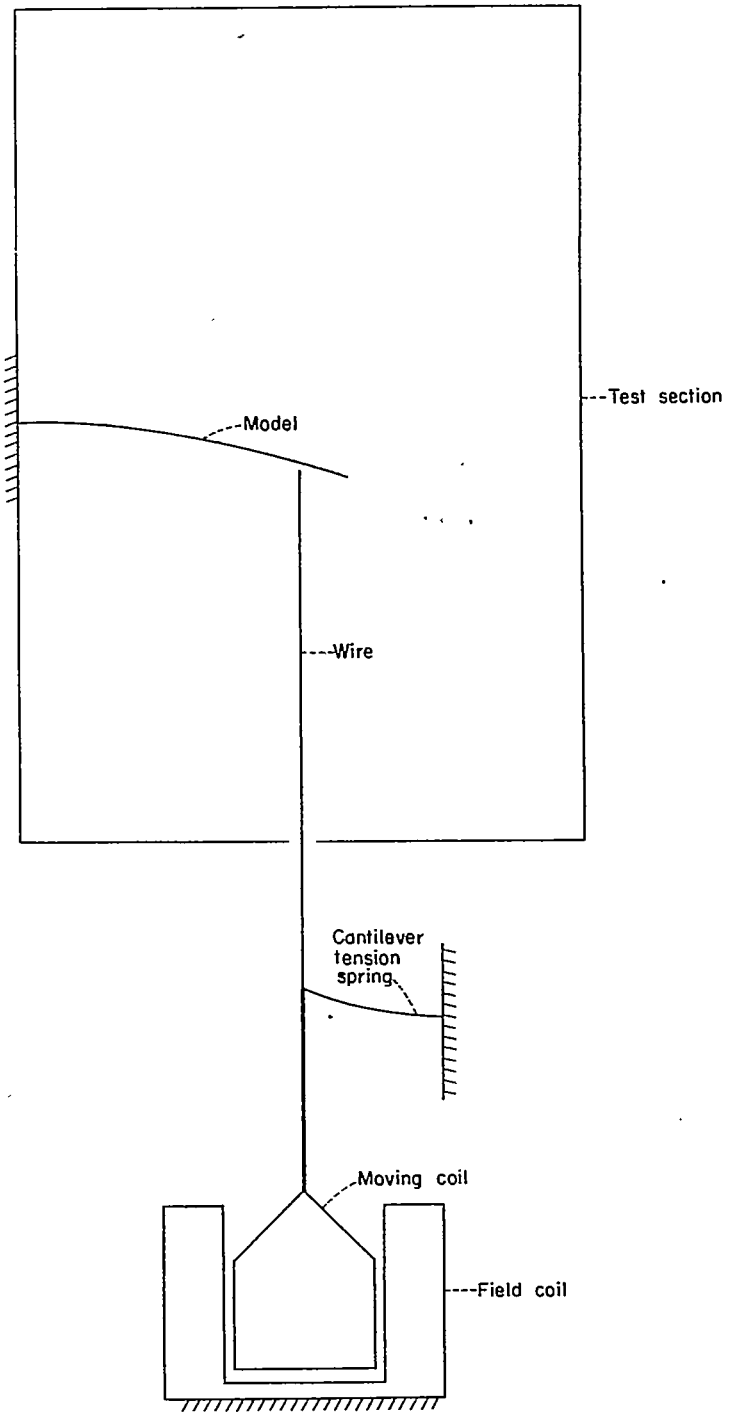

FIGURE 17.—Schematic drawing of test setup for three-dimensional measurements.

A variable-frequency voltage was supplied to the shaker by a low-frequency oscillator and a power amplifier. The voltage across the coil of the shaker was measured by use of a vacuum-tube voltmeter. The current through the coil was measured by use of a vacuum-tube voltmeter shunted with a 1-ohm precision resistor. The power consumed by the shaker was measured by use of a low-power-factor wattmeter.

A photograph of the research instrument console used in the Langley 2- by 4-foot flutter research tunnel is shown in figure 20.

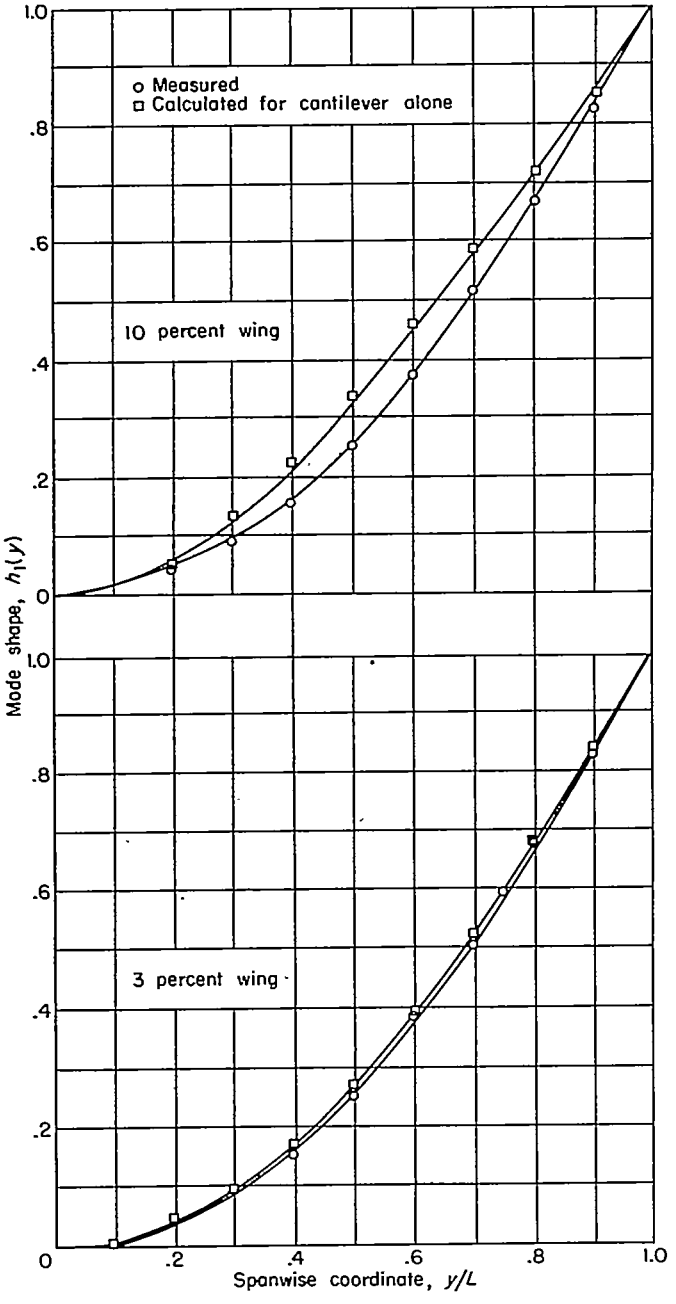

FIGURE 18.—Comparison of actual bending modes for three-dimensional tests with calculated fundamental bending modes for same wings as ideal cantilevers.

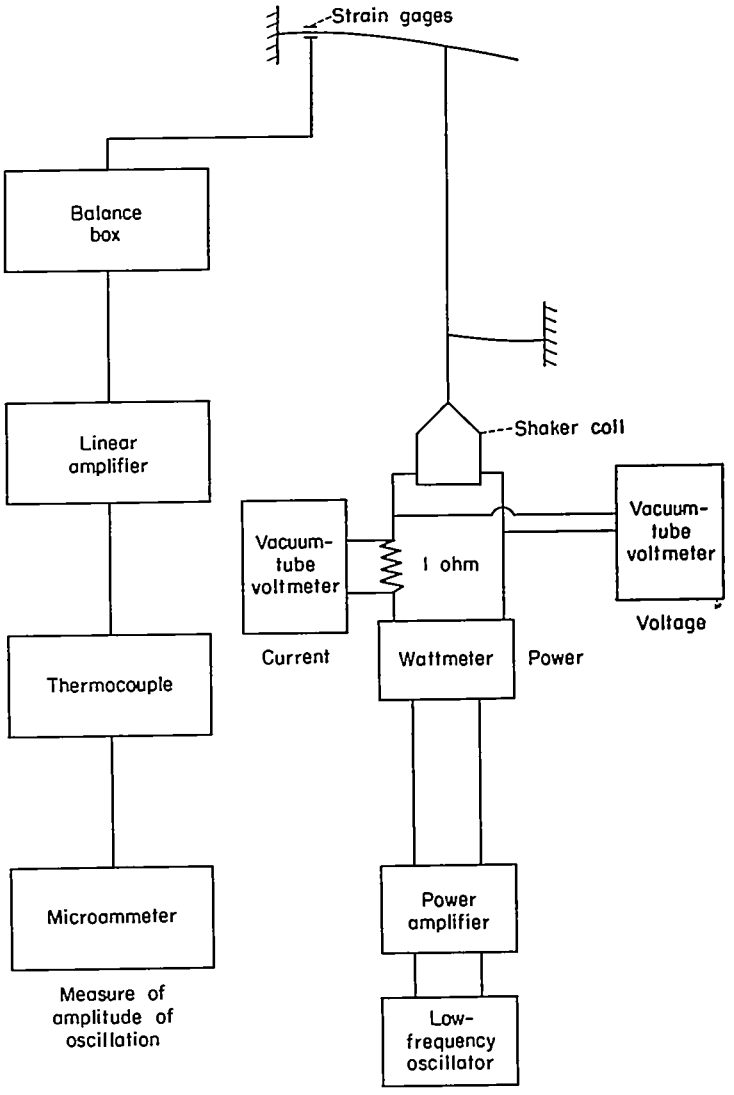

FIGURE 19.—Block diagram of instrumentation used for three-dimensional tests.

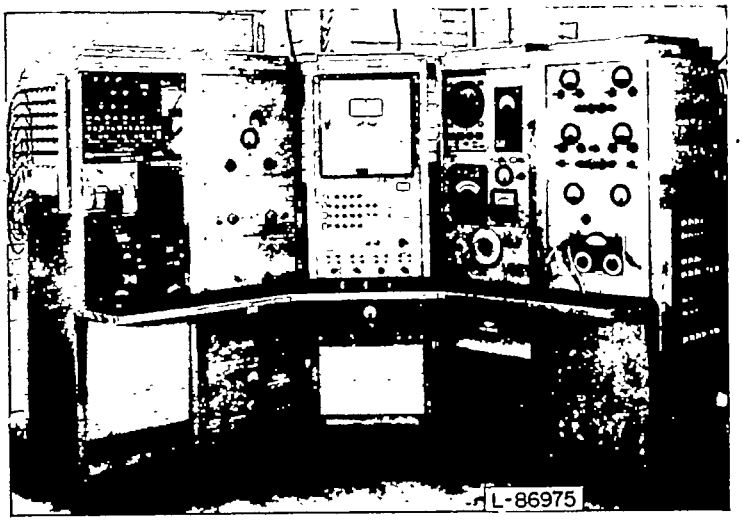

FIGURE 20.—Photograph of research instrument console used in Langley 2- by 4-foot flutter research tunnel.

PROCEDURE

The procedures used in determining the aerodynamic damping in the bending mode were essentially the same for the two finite-span wings except that the data for the 10-percent wing were obtained at fixed velocities with angle of attack as the primary variable, whereas the data for the 3-percent wing were obtained at constant angles of attack with velocity as the primary variable.

The procedure used in the tests of the 10-percent wing was as follows: After the desired velocity had been set, the mean angle of attack was adjusted by a motor-driven angle-of-attack changing and clamping device. The frequency of the oscillator was varied until the system was tuned to the frequency of maximum response. The power to the electromagnetic shaker was adjusted to bring the amplitude of oscillation to the desired level as indicated by a mean-square root-bending-strain indicator. The desired voltage, current, and power were then observed.

The preceding procedure was repeated in increments of mean angle of attack of about 2° up to 20°. Because of the occurrence of stall flutter in a torsion mode, the limiting angle of attack at the higher velocities was less than 20°.

Essentially, the same procedure was followed for the 3-percent wing except that, at each angle of attack, measurements were made at several velocities before the angle was changed.

The aerodynamic-damping coefficients for bending oscillations of the 10-percent and the 3-percent wings were determined at several values of reduced frequency by varying the flow velocity. The tests were conducted at atmospheric pressure in air. The variations of Mach number, Reynolds number, and tip angularity with reduced velocity (the reciprocal of reduced frequency) for the two wings are shown in figure 21.

DATA REDUCTION

For clarity, a somewhat simplified presentation of the relationships involved in reducing the data is developed here. A more detailed presentation is made in appendix D.

The actual distributed system used for the three-dimensional measurements is replaced by an equivalent single-degree-of-freedom system which has the following equation of motion:

$$M_e\ddot{h}+(C_a+C_s)\dot{h}+K_eh=F(t) \tag{1}$$

where h is the bending deflection of the wing and the coefficients M_e and K_e represent the generalized mass and stiffness, respectively. The coefficients C_a and C_s refer to the aerodynamic and structural damping, respectively. The

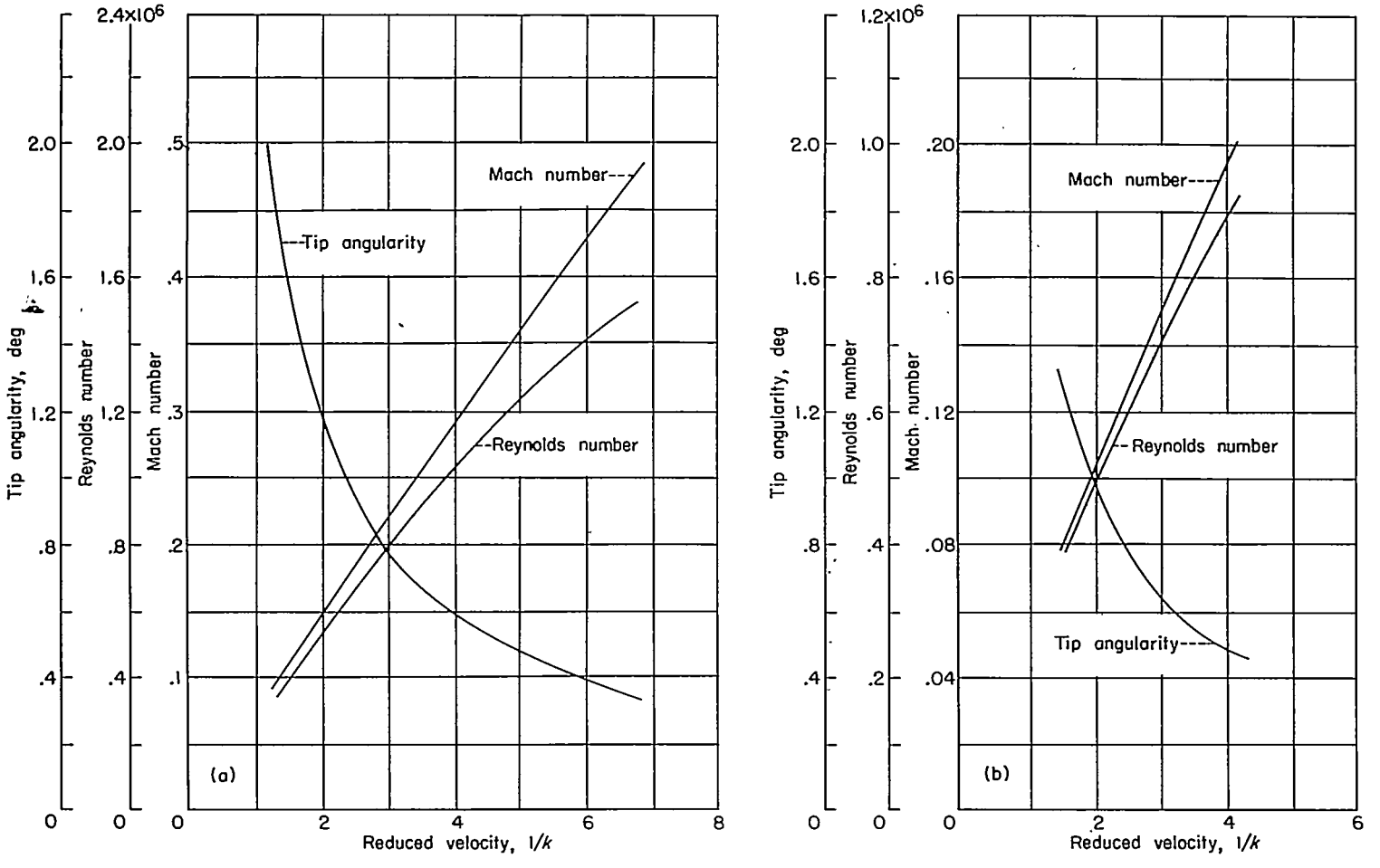

(a) 3-percent-thick wing (b) 10-percent-thick wing.

FIGURE 21.—Variation of Mach number, Reynolds number, and tip angularity with reduced velocity for finite-span models.

external force $F(t)$ is again composed of three parts: a steady-state force associated with the mean angle of attack $\bar{\alpha}$, a sinusoidal force F_0, and a random force F_R. The steady-state force leads only to a static deflection of the beam and consequently will not be treated further.

Equation (1) may be rewritten as

$$M_e(\ddot{h}_0+\ddot{h}_R)+(C_a+C_s)(\dot{h}_0+\dot{h}_R)+K_e(h_0+h_R)=F_0+F_R \quad (2)$$

where the subscripts 0 and R refer to quantities related to the forces F_0 and F_R, respectively.

Multiplying equation (2) by F_0 and taking time averages yields

$$M_e\overline{\ddot{h}_0F_0}+M_e\overline{\ddot{h}_RF_0}+(C_a+C_s)\overline{\dot{h}_0F_0}+(C_a+C_s)\overline{\dot{h}_RF_0}+K_e\overline{h_0F_0}+K_e\overline{h_RF_0}=\overline{F_0^2}+\overline{F_RF_0}$$

where bars over the quantities refer to a time average over an arbitrary period of time T. However,

$$M_e\overline{\ddot{h}_RF_0}=0$$
$$(C_a+C_s)\overline{\dot{h}_RF_0}=0$$
$$K_e\overline{h_RF_0}=0$$
$$\overline{F_RF_0}=0$$

as $T\to\infty$ because the time average of the product of two uncorrelated quantities is zero. Also, at the natural frequency of the system, the sum of kinetic and potential forces must be zero; this fact leads to the condition that

$$M_e\overline{\ddot{h}_0F_0}+K_e\overline{h_0F_0}=0$$

Therefore,

$$(C_a+C_s)\overline{\dot{h}_0F_0}=\overline{F_0^2}$$

or

$$C_a=\frac{\overline{F_0^2}}{\overline{\dot{h}_0F_0}}-C_s$$

Critical damping of the system is defined as

$$C_{cr}=2\omega_1M_e$$

where ω_1 is the first natural frequency of the system and is related to the stiffness and mass by the following equation:

$$\omega_1^2=\frac{K_e}{M_e}$$

Then, the ratio of aerodynamic damping to critical damping may be defined as

$$\frac{C_a}{C_{cr}}=\frac{\overline{F_0^2}}{\overline{\dot{h}_0F_0}}\frac{1}{2\omega_1M_e}-\frac{C_s}{C_{cr}}$$

The aerodynamic-damping ratio can be determined by measuring the current through the shaker coil which is proportional to F_0 and by measuring the power consumed by the system which is proportional to the product $\dot{h}F_0$. The structural-damping ratio was measured in still air before each test so that it could be subtracted from the values measured during the test.

Of course, certain corrections are required, and certain approximations are involved in converting the measured electrical quantities to the desired damping coefficient. For example, the electrical-power losses in the shaker coil must be extracted as a tare. In addition, the random force F_R produces random velocities of the coil $\dot{h}_R$ which, in turn, induce correlated voltages and currents in the electrical system. These currents are small, however, if the driving coil is excited by a high impedance generator.

The ratios of aerodynamic damping to critical damping obtained in this manner apply only to the particular mechanical systems used in these experiments. In order to make the damping measurements of more general value, the ratios of aerodynamic damping to critical damping were used to determine an effective section derivative F_e having the same form as Theodorsen's circulation function $F(k)$. (See ref. 17.) The relationship between the damping ratio and the effective aerodynamic-damping coefficient is developed in appendix D. The derivative F_e is defined as

$$F_e=\frac{k\frac{C_a}{C_{cr}}}{\kappa_e\cos\bar{\alpha}} \quad (3)$$

where k is the reduced frequency based on the chord at the three-quarter semispan and κ_e is a mass-ratio parameter shown in appendix D. Values of F_e determined in this manner represent an effective or weighted section derivative which may be used in a strip-analysis estimation of damping in the bending mode for wings having geometric properties similar to the two tested in this investigation.

RESULTS AND DISCUSSION

The measured ratios of aerodynamic damping to critical damping in the bending mode for the 10-percent wing are shown in figure 22 as functions of angle of attack for various values of reduced frequency. The damping ratios for the 3-percent wing are shown in figure 23 as functions of reduced velocity for various angles of attack. The effective aerodynamic-damping coefficients in the bending mode F_e for both the 10-percent and the 3-percent wings are shown in figures 24 and 25 as functions of reduced frequency at various angles of attack.

LOW ANGLES OF ATTACK

As a matter of reference, Theodorsen's theoretical two-dimensional circulation function F(k) (ref. 17) is shown in figures 24 and 25 which are plots of the measured effective aerodynamic-damping coefficients for bending oscillations as functions of reduced frequency. As might be expected, the data for these relatively low-aspect-ratio wings at the lower mean angles of attack generally fall considerably below the values of F_e indicated by the two-dimensional theory.

The data for the 10-percent and the 3-percent wings are generally similar at the low angles of attack, except at low values of reduced frequency.

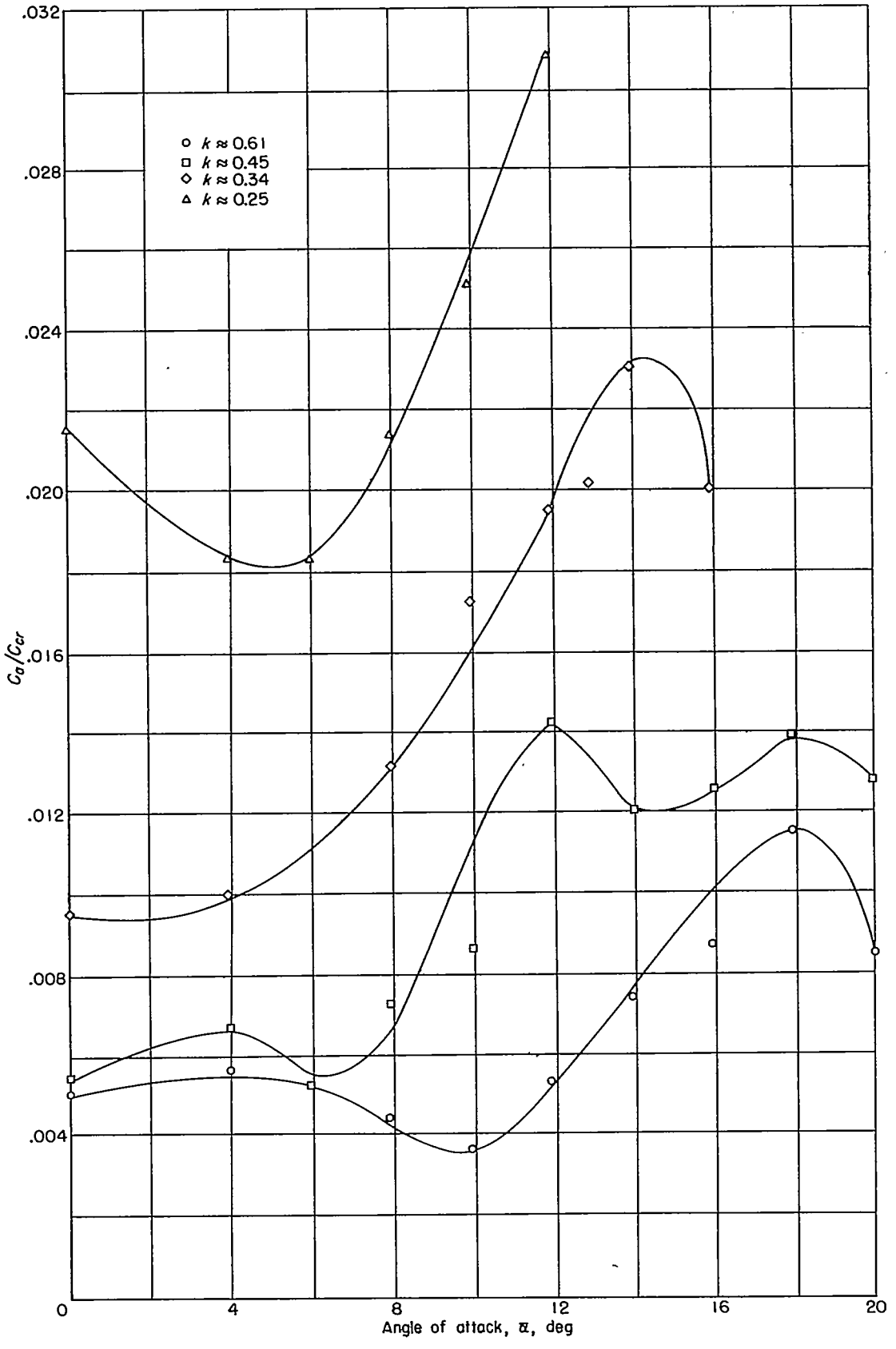

FIGURE 22.—Variation of aerodynamic-damping ratio for bending oscillations with angle of attack for 10-percent-thick wing.

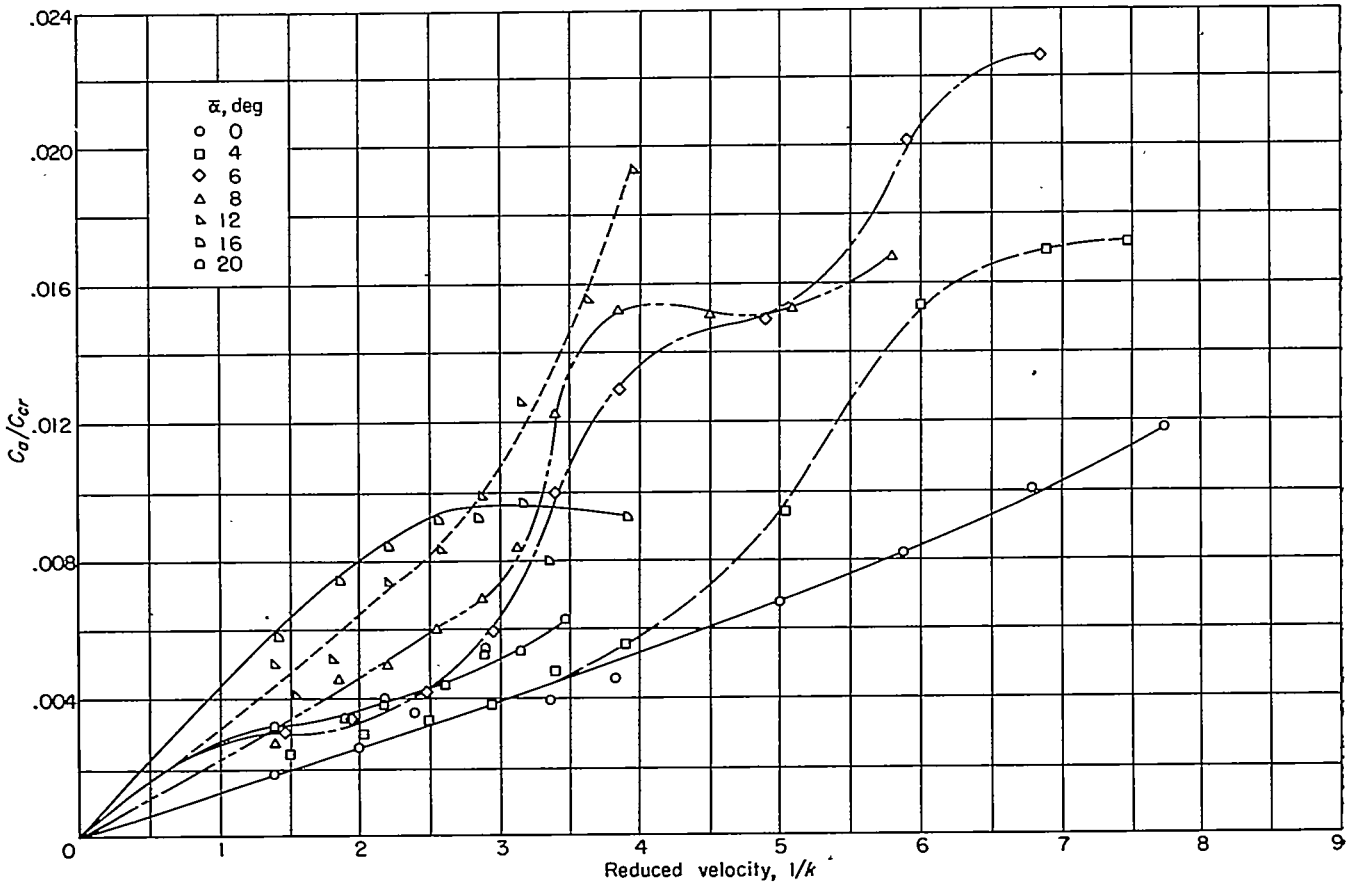

FIGURE 23.—Variation of aerodynamic-damping ratio for bending oscillations with reduced velocity for 3-percent-thick wing.

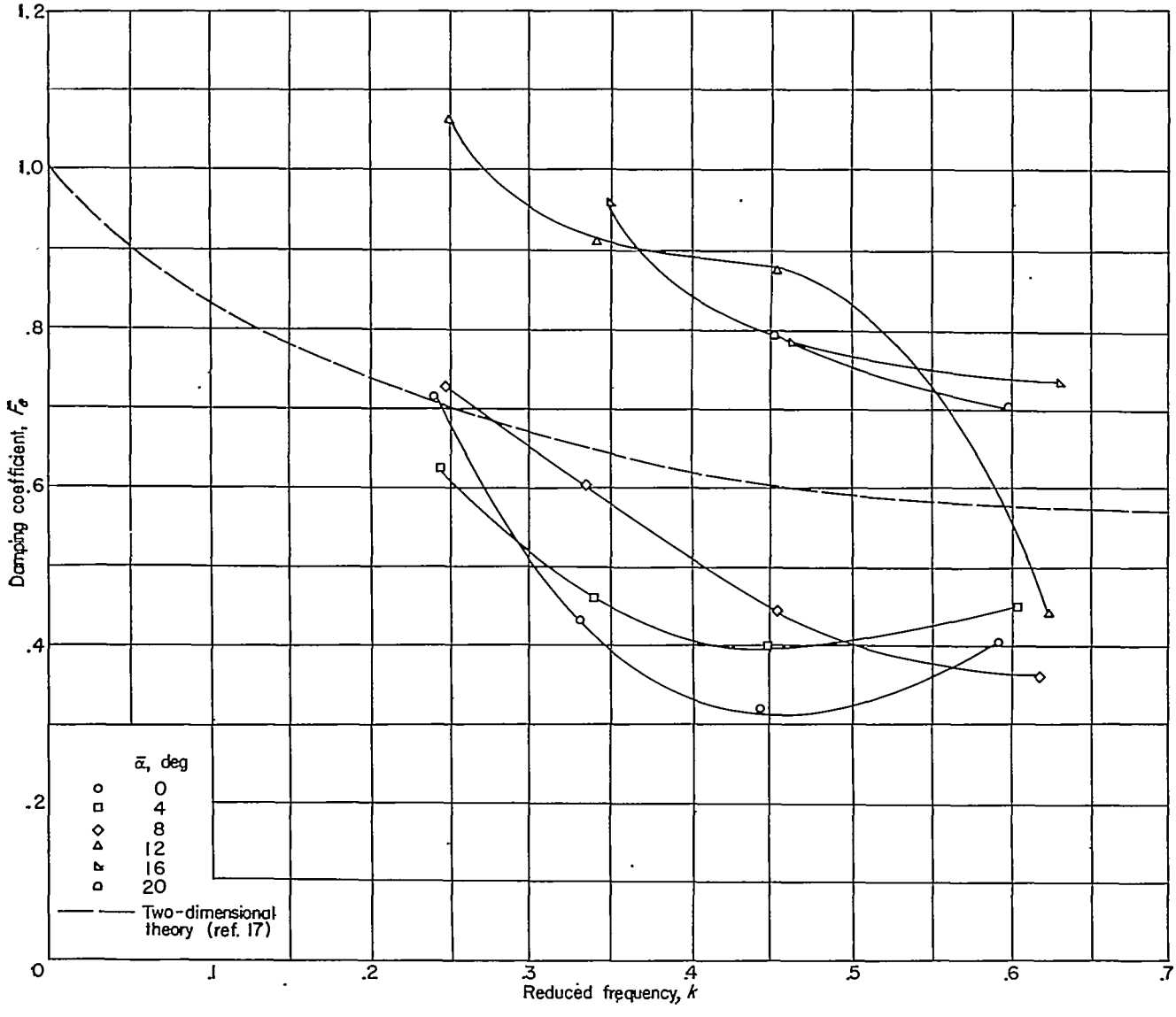

FIGURE 24.—Effective aerodynamic-damping coefficient for bending oscillations for 10-percent-thick wing.

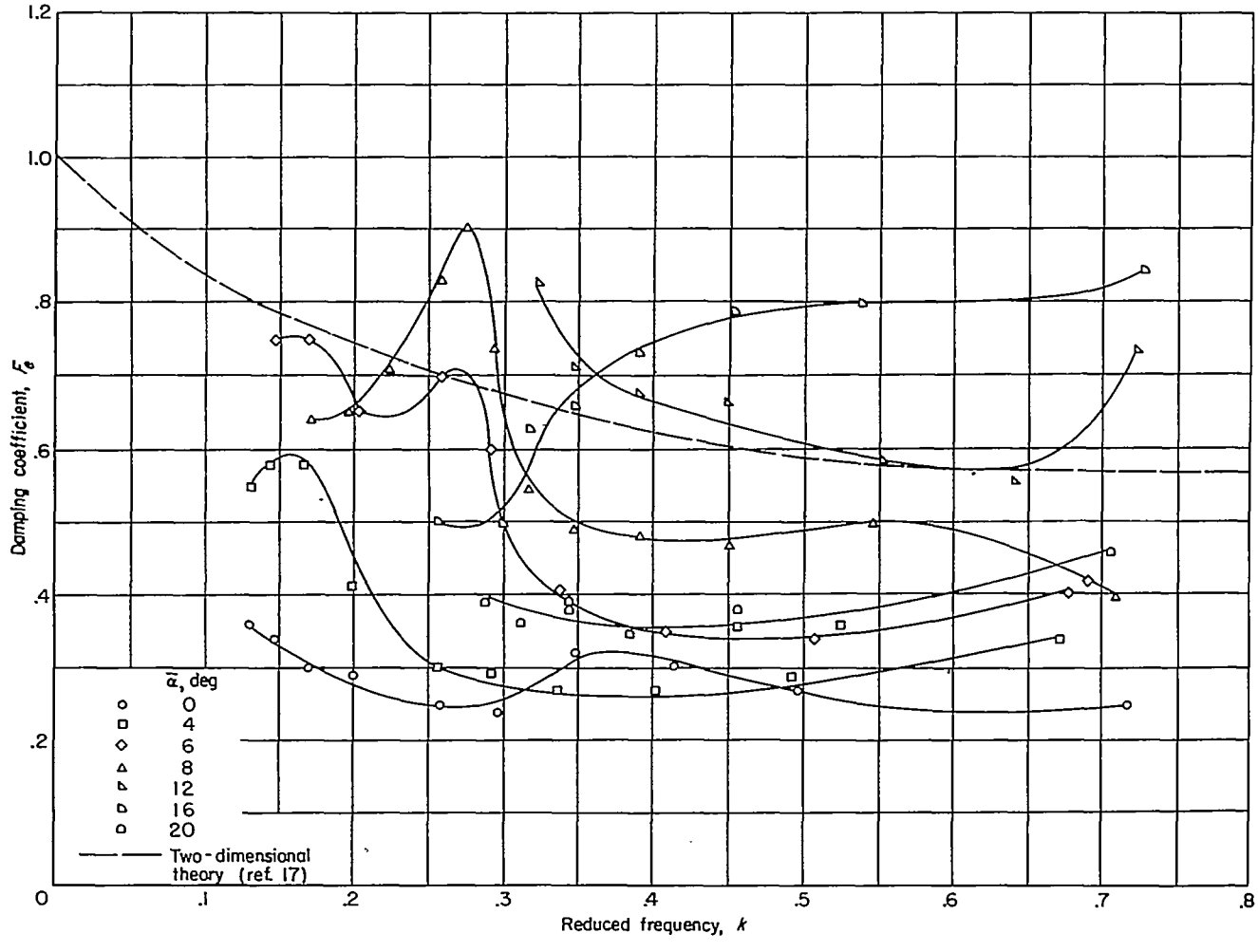

FIGURE 25.—Effective aerodynamic-damping coefficient for bending oscillations for 3-percent-thick wing.

HIGH ANGLES OF ATTACK

In general, the outstanding characteristic of the damping measurements for bending oscillations presented in figures 22 to 25 is the increased positive damping which occurred at the higher mean angles of attack. Within the range of angle of attack and reduced frequency covered by these experiments, the damping in the bending mode remained positive for all conditions; and at some conditions, the damping at high mean angles of attack was as much as about three times the damping at zero angle of attack.

This increase in damping of the bending mode at high mean angles of attack may be related to the increase in the magnitude of normal-force and pitching-moment coefficients which was observed for the two-dimensional wing oscillating in pitch. However, for the pitching motion the increase in magnitudes was accompanied by changes in phase angle which produced negative damping moments. This difference in damping characteristics is not inconsistent with the results obtained for the bending measurements since the phase relationships which determine aerodynamic damping are very different for the two types of motion. Generally speaking, in the frequency range of practical interest, the predominant source of aerodynamic force or moment for a pitching wing is associated with the position terms, whereas in the case of bending oscillations the predominant source is associated with the velocity terms.

CONCLUSIONS

The magnitude and phase of the fundamental components of normal force and pitching moment acting on an NACA 65A010 airfoil oscillating in pitch about the midchord have been measured at both high and low mean angles of attack at Mach numbers of 0.35 and 0.7. In addition, the aerodynamic damping in, essentially, the first bending mode has been measured for two finite-span wings over a range of mean angles of attack and reduced frequency. Examination of the results of this investigation indicate the following significant conclusions:

1. The magnitudes of oscillatory normal-force and pitching-moment coefficients for a two-dimensional wing oscillating in pitch about the midchord at high mean angles of attack are much larger at some conditions than at low mean angles of attack.

2. Large regions of angle of attack and reduced frequency exist wherein a single-degree-of-freedom torsion flutter is possible because of unstable aerodynamic-damping moments for pitching oscillations.

3. The effect of increasing Mach number from 0.35 to 0.7 was to decrease the initial angle of attack at which unstable damping occurred.

4. The aerodynamic damping for bending oscillations was generally higher at high angles of attack than at low angles of attack, and no unstable damping was encountered over the range of configurations, angle of attack, and reduced frequency covered by these experiments.

LANGLEY AERONAUTICAL LABORATORY,
NATIONAL ADVISORY COMMITTEE FOR AERONAUTICS,
LANGLEY FIELD, VA., *January 21, 1956.*

APPENDIX A

EFFECTS OF LEADING-EDGE CONDITIONS ON AERODYNAMIC DAMPING FOR AIRFOIL OSCILLATING IN PITCH

The effects of two types of disturbances placed at the leading edge of an airfoil oscillating in pitch were determined at a Mach number of 0.35 and angles of attack of 8° and 12°. The two types of disturbances which were chosen for study were a leading-edge roughness which consisted of a sprinkling of No. 120 carborundum grains over the leading 4 percent of the chord and a tripper-wire configuration which consisted of a wire about 0.4 percent of the chord in diameter located on the upper surface at 5 percent of the chord rearward of the leading edge. The magnitude and phase angle of the fundamental component of pitching moment were measured. The damping-moment coefficients obtained at the two mean angles of attack tested are shown in figure 26 along with the values obtained for the clean airfoil.

At a mean angle of attack of 8°, the effect of the changes in leading-edge condition is pronounced. The damping coefficients for the leading-edge-roughness tests reach considerably larger unstable values and the crossover point between stable and unstable values occurs at a much higher value of reduced frequency. The data for the tripper-wire tests at $\bar{\alpha}=8°$, on the other hand, indicate some improvement over the clean airfoil. The conventional static-pitching-moment coefficients have been measured for the three airfoil conditions and are shown in figure 27. It appears that the addition of the tripper wire to the upper surface of the airfoil increased the angle of attack at which the maximum static-pitching-moment coefficient occurred from about 9° to about 10°, whereas the addition of the leading-edge roughness decreased the angle of maximum moment to about 8°. It appears, therefore, that the severity of unstable damping in this case depends upon the nearness of the mean angle of attack to the angle of attack at which maximum static pitching moment occurs. The damping moments measured at $\bar{\alpha}=12°$, shown in figure 26, are relatively unaffected by the condition of the leading edge. This insensitivity, presumably, is due to the fact that at $\bar{\alpha}=12°$ the airfoil is well beyond the angle of maximum moment (as indicated in fig. 27) for all three conditions.

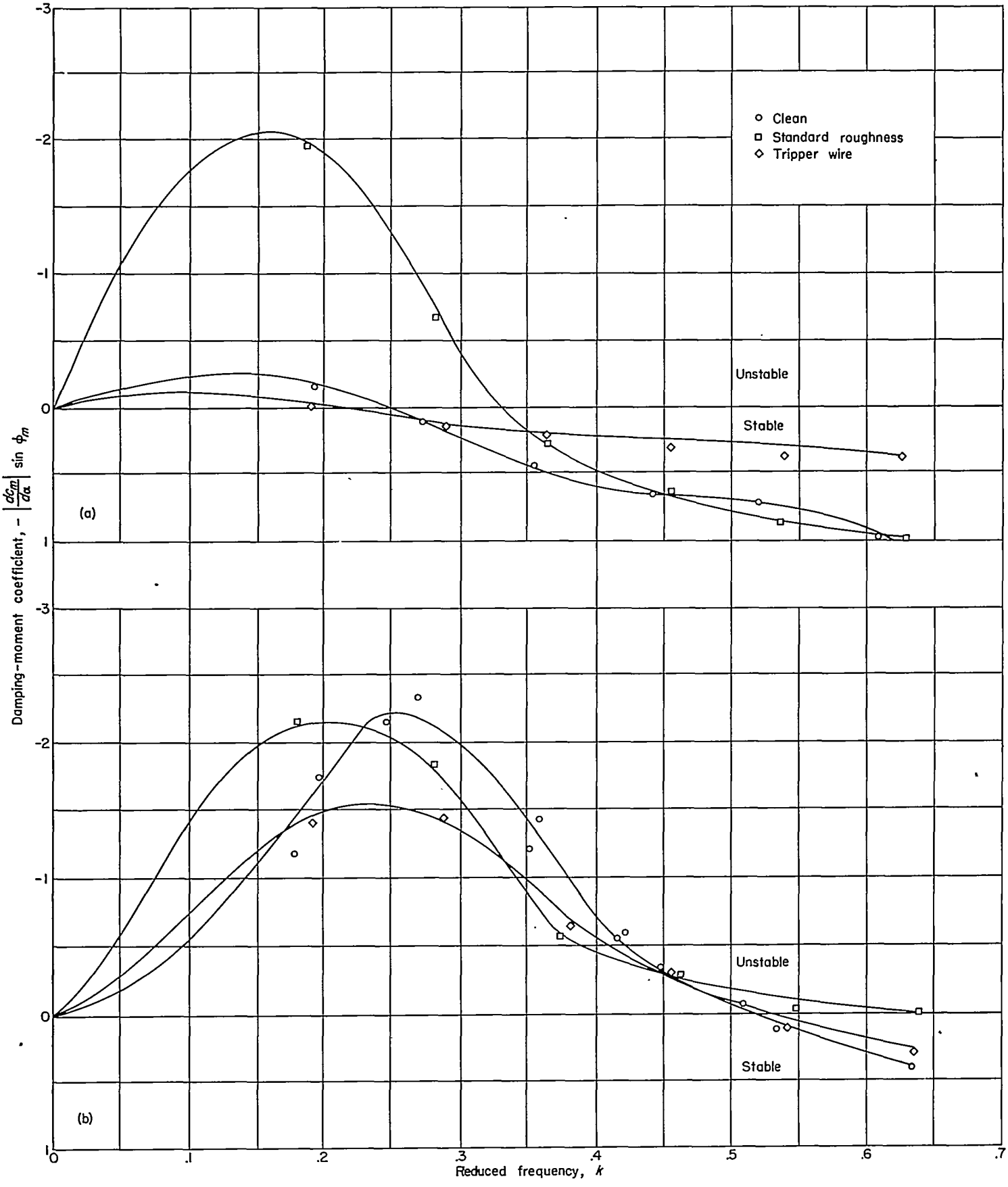

(a) $\bar{\alpha}=8°$.
(b) $\bar{\alpha}=12°$.

FIGURE 26.—Variation of damping-moment coefficients with reduced frequency for 65A010 airfoil having three different leading-edge conditions.

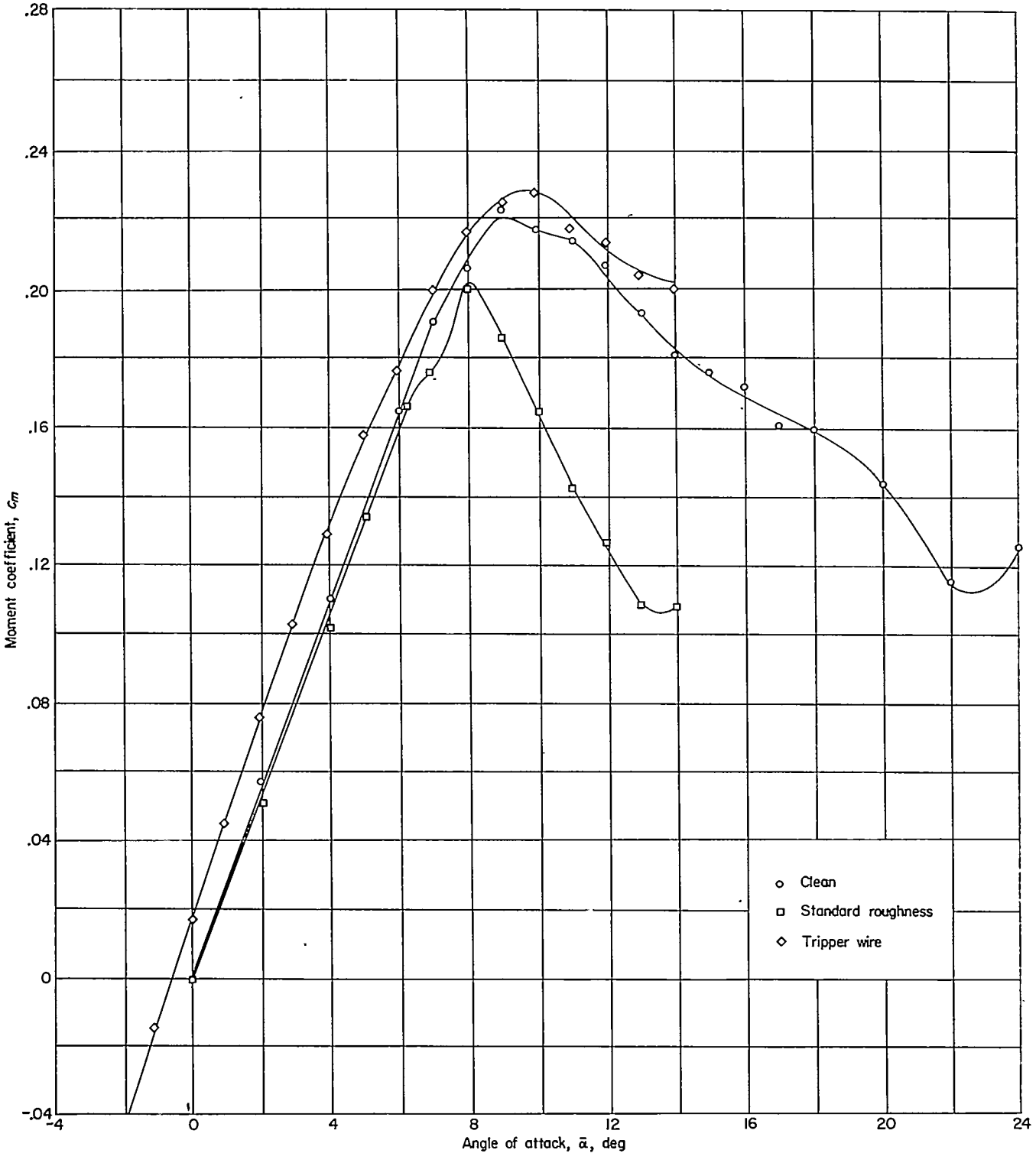

FIGURE 27.—Variation of static-pitching-moment coefficient with angle of attack for 65A010 airfoil having different leading-edge conditions.

APPENDIX B

SOME OBSERVATIONS ON TIME HISTORIES OF INDIVIDUAL PRESSURES ON AN OSCILLATING AIRFOIL NEAR STALL

Numerous investigators have attempted to formulate an analytical approach to the prediction of unsteady air forces for wings oscillating near the stall. Since this problem inherently involves the complexities of unsteady boundary-layer behavior, almost all the approaches have been empirical in the sense that experimentally observed phenomena have been utilized in formulating the necessary assumptions. So far, these analytical calculations have yielded satisfactory results for only limited ranges of the various parameters. One contributing cause of this lack of a satisfactory analytical approach is that the phenomena involved in the process have not been completely described experimentally. In order to contribute further to the store of knowledge concerning oscillating air forces for stalled wings, some additional information obtained during the course of the investigation of the NACA 65A010 airfoil pitching about the midchord is included.

At a Mach number of 0.35 and Reynolds number of 5.3×10^6, a unique condition was encountered at angles of attack near 8°. A series of short samples of oscillographic records of the individual pressures is reproduced in figure 28. At an angle of attack of 6.8° and at zero frequency, the incremental pressures over the wing were relatively undisturbed except for some small variations which occurred near the trailing edge. As the angle of attack was slowly increased, intermittent pressure fluctuations occurred near the leading edge at angles of attack above about 7.6°. This condition is illustrated in figure 28 (b) for an angle of attack of 8° and zero frequency. As the angle of attack was further increased, all the pressure gages indicated a continuous random fluctuation which is illustrated in figure 28 (c) for an angle of attack of 9.2°.

When the airfoil was oscillated in pitch about the midchord at a mean angle of attack of 8°, this pattern of flow breakdown indicated by the random fluctuations in pressure was maintained in the sense that the flow periodically broke down as the angle of attack was periodically increased. The primary effect of the oscillation appeared to be a delay in the instantaneous angle of attack at which the flow breakdown began. At a reduced frequency of 0.073, the gage nearest the leading edge indicated a disturbance commencing at an angle of attack of about 7.8° which represents a time delay of about 6 milliseconds beyond the time at which the airfoil reached 7.6° (the angle at which flow breakdown began for static conditions). At a reduced frequency of 0.270, the angle of attack at which flow fluctuation began was delayed to about 8.5° which corresponds to a time delay of about 8 milliseconds.

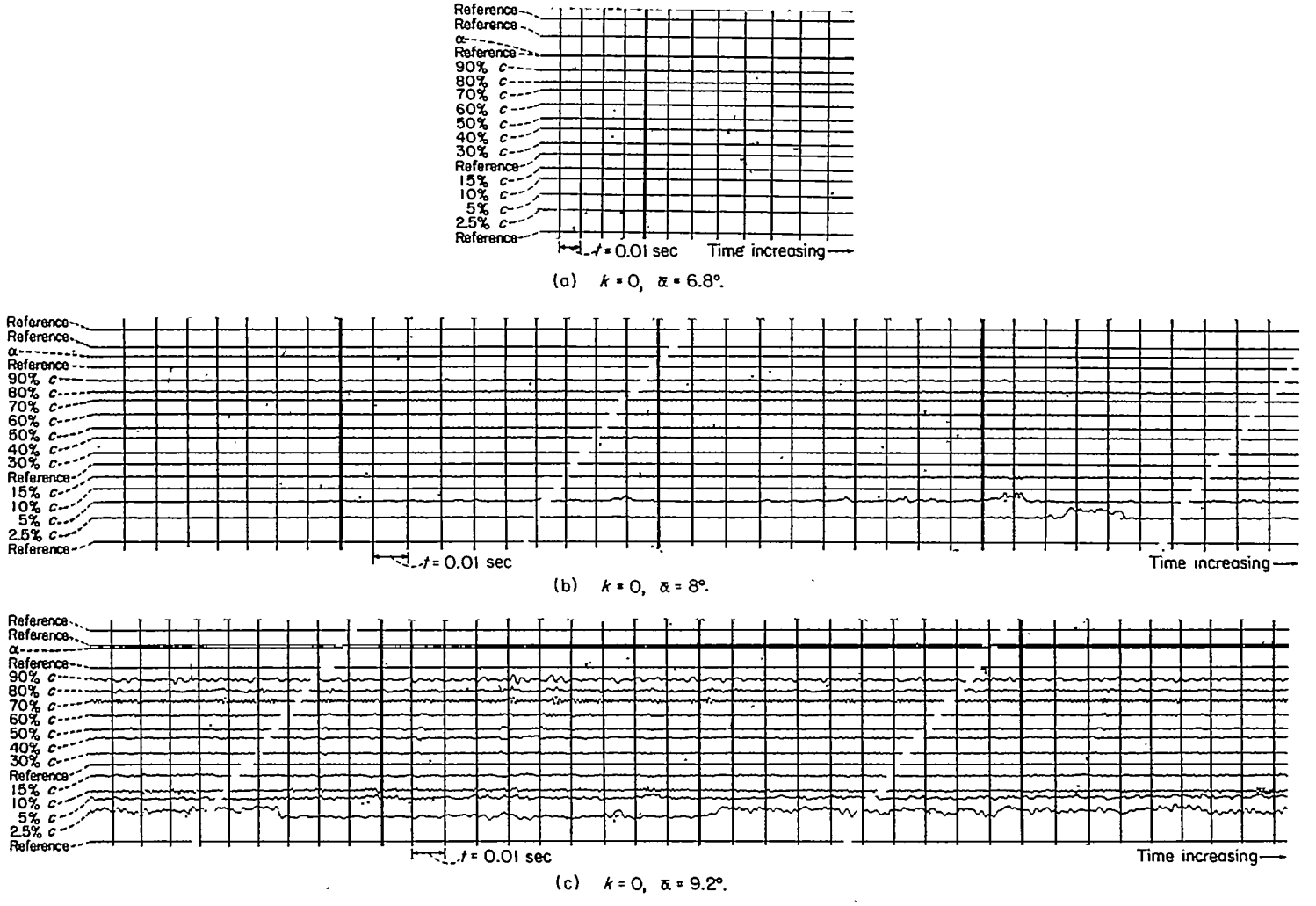

(a) $k = 0$, $\bar{\alpha} = 6.8°$.

(b) $k = 0$, $\bar{\alpha} = 8°$.

(c) $k = 0$, $\bar{\alpha} = 9.2°$.

FIGURE 28.—Time-history records of individual pressures of 65A010 airfoil oscillating in pitch at Mach number of 0.35. Positive pressure and positive angle of attack is up.

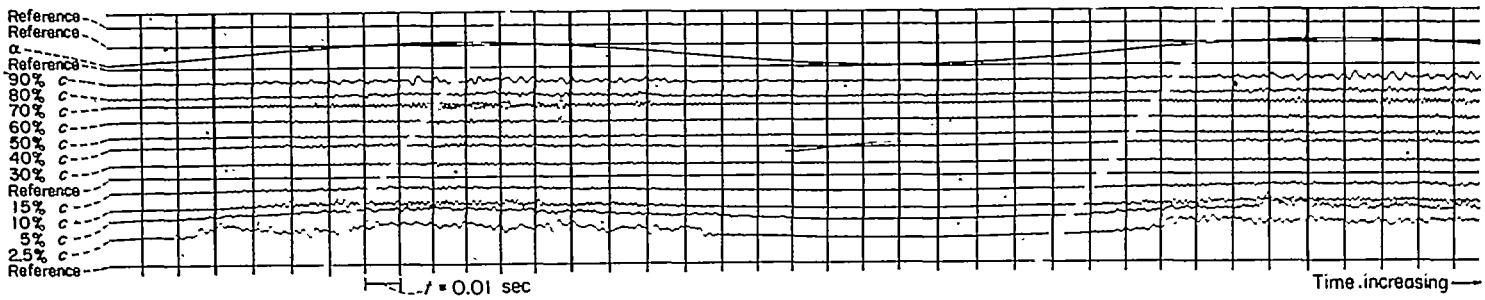

(d) $k = 0.073$, $\bar{\alpha} = 8°$.

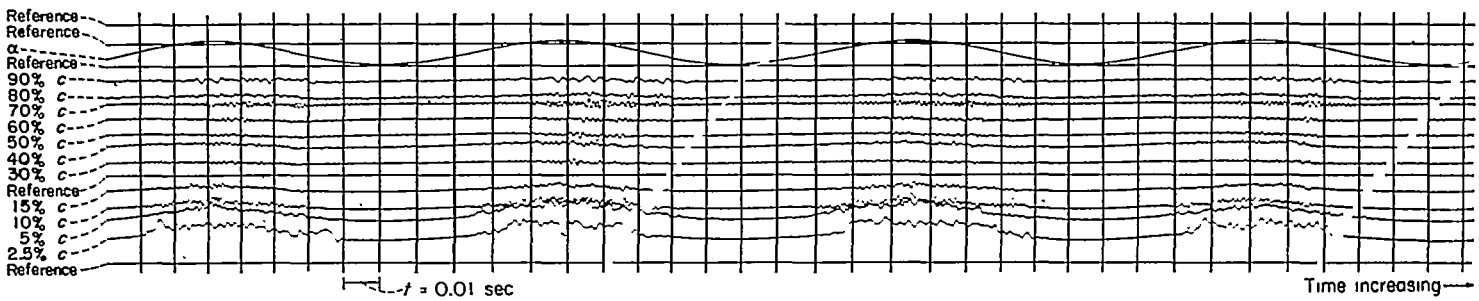

(e) $k = 0.183$, $\bar{\alpha} = 8°$.

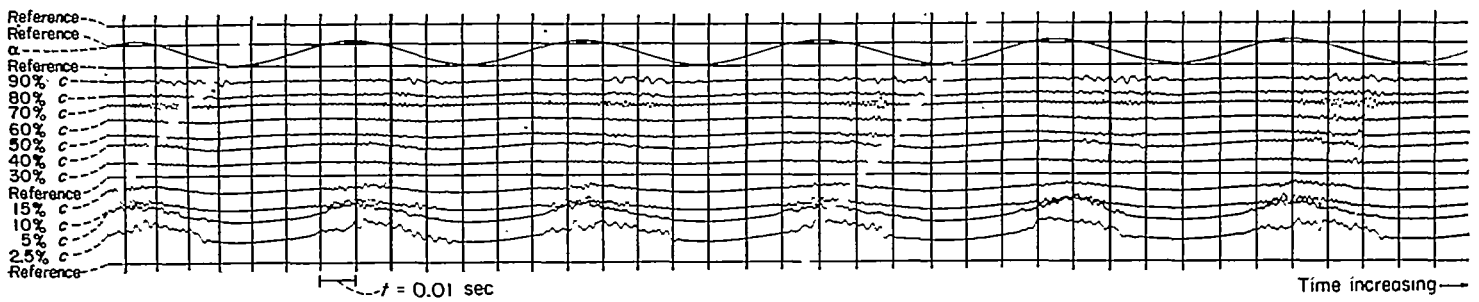

(f) $k = 0.270$, $\bar{\alpha} = 8°$.

FIGURE 28.—Concluded.

APPENDIX C

SOME REMARKS CONCERNING NONLINEARITIES IN AERODYNAMIC FORCES

The possibility of nonlinear aerodynamic effects in stall flutter and buffeting cannot be ignored. For linear systems, once the instability point has been passed, a divergent oscillation occurs. In stall flutter, however, it has been observed that the oscillations will usually reach an equilibrium amplitude for fixed conditions. Sisto (ref. 1) has pointed out that any attempt to estimate amplitudes of stall flutter must consider the nonlinear aspects of the phenomena. In buffeting studies of the type proposed by Liepmann (refs. 5 and 6), it is necessary to assume that the system is linear. Thus, the problem of determining the nonlinear characteristics of oscillating air forces for stalled wings is important.

In the present investigation, a few limited studies of the nonlinearity of the oscillatory air forces have been made. Two different techniques were employed. For the 10-percent-thick wing oscillating in the first bending mode, the aerodynamic damping was measured as a function of amplitude of oscillation. For the two-dimensional wing, the oscillatory normal forces and pitching moments at several conditions were examined for harmonic content.

If a wing oscillates in simple harmonic motion, nonlinearities in the aerodynamic forces should cause higher harmonics to appear in the oscillatory air forces. Since the amplitude of oscillation of the two-dimensional wing could not easily be varied, the harmonic-content method of studying the nonlinearities was adopted. At several conditions of angle of attack and frequency, the electrical signals proportional to normal force or pitching moment were scanned by tuning the narrow band-pass filter through its frequency range. No significant harmonic content was noted for any of the conditions examined. Figure 6 is representative of the results obtained. Since the amplitude of oscillation used in the two-dimensional tests was relatively small (nominally $\pm 1.2°$), it is possible that the nonlinearities which may have existed were not sufficiently large to be detected by the method used.

The results obtained for the 10-percent-thick wing oscillating in the bending mode at various tip amplitudes are shown in figure 29 where the aerodynamic-damping ratio is plotted as a function of tip amplitude for various angles of attack at a reduced frequency of about 0.35. The range of tip amplitudes covered in this experiment represents a tip angularity from $\pm 0.66°$ to $\pm 2.3°$. The data do not indicate any particular trend of aerodynamic damping with amplitude; however, there are differences of about 25 percent at various amplitudes. The significance of differences of this size would, of course, depend upon the nature of the calculation in which the damping values might be used.

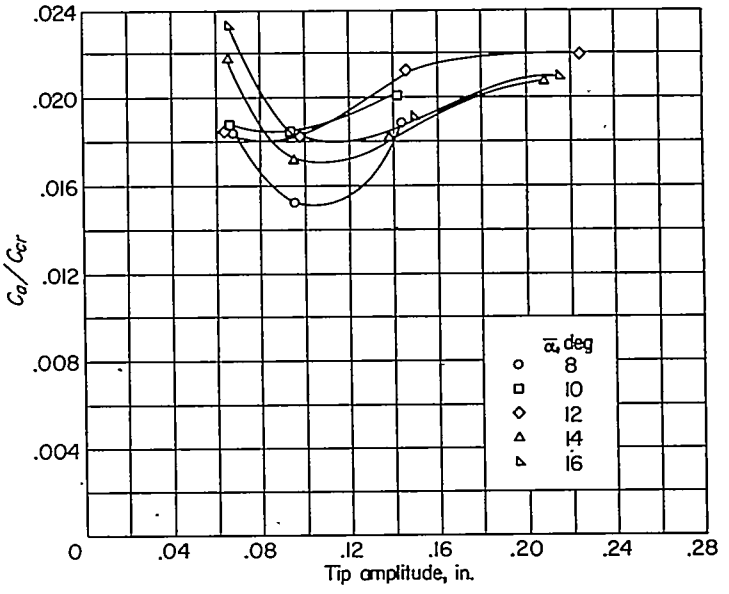

FIGURE 29.—Variation of aerodynamic-damping ratio for 10-percent-thick wing with amplitude of oscillation. $k \approx 0.35$.

APPENDIX D

DEVELOPMENT OF DATA-REDUCTION RELATIONS FOR FINITE-SPAN WINGS OSCILLATING IN FIRST BENDING MODE

The more important features of the method employed to deduce the desired nondimensional coefficients of aerodynamic damping for the finite-span wings oscillating in the first bending mode were presented in the text. The purpose of this appendix is to present the development of some of the relations used in reducing the data in somewhat more detail. Some of the features of the method which are presented in the text (such as the manner of accounting for the random force) are not included.

The system is a cantilever beam which has attached to it at the spanwise coordinate y_c an external mass M_c and external spring K_c. The external mass and spring act on the beam through the mean angle of attack $\bar{\alpha}$ as indicated in sketches 1 and 2. The system is excited by a vertical

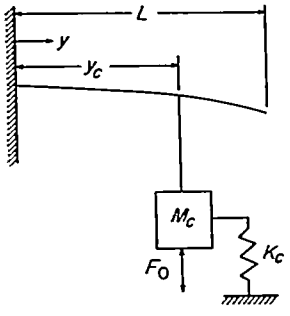

Sketch 1

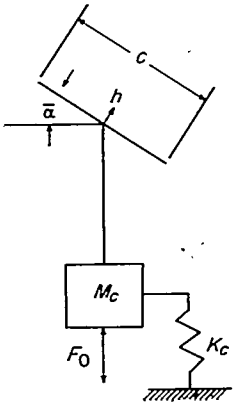

Sketch 2

sinusoidal force $F_0e^{i\omega t}$ which also acts upon the beam through the angle $\bar{\alpha}$. It is assumed that the motion of the beam is confined to one degree of freedom, namely, the first bending mode of the system which is defined as $h=a_1h_1(y)$ where h is the bending deflection of the beam normal to the chord, a_1 is the tip deflection, and $h_1(y)$ is the first-bending-mode shape expressed in terms of a unit tip deflection. The following development is similar to that in reference 18.

The potential energy of this system is

$$E_p=\frac{1}{2}\int_0^L EI\left\{\frac{\partial^2}{\partial y^2}[a_1h_1(y)]\right\}^2dy+\frac{1}{2}K_c\left[a_1h_1(y_c)\cos\bar{\alpha}\right]^2 \quad \text{(D1)}$$

The effective stiffness of the beam in the first bending mode is defined as

$$K_{h_1}=\int_0^L EI\left\{\frac{\partial^2}{\partial y^2}[h_1(y)]\right\}^2dy$$

Thus, equation (D1) becomes

$$E_p=\frac{1}{2}a_1^2K_{h_1}+\frac{1}{2}a_1^2K_c\,[h_1(y_c)\cos\bar{\alpha}]^2$$

$$=\frac{1}{2}a_1^2K_e$$

The kinetic energy of the system is

$$E_t=\frac{1}{2}\dot{a}_1^2\int_0^L m[h_1(y)]^2dy+\frac{1}{2}\dot{a}_1^2M_c\,[h_1(y_c)\cos\bar{\alpha}]^2 \quad \text{(D2)}$$

The effective mass of the beam in the first bending mode is defined as

$$M_{h1}=\int_0^L m[h_1(y)]^2dy$$

and equation (D2) becomes

$$E_t=\frac{1}{2}\dot{a}_1^2M_{h_1}+\frac{1}{2}\dot{a}_1^2M_c[h_1(y_c)\cos\bar{\alpha}]^2$$

$$=\frac{1}{2}\dot{a}_1^2M_e$$

If the assumption of viscous damping for the system is made, the structural damping is described by the dissipation function which is defined as

$$D=\frac{1}{2}\dot{a}_1^2\int_0^L C\,[h_1(y)]^2dy$$

or

$$D=\frac{1}{2}\dot{a}_1^2C_e$$

The virtual work δW done by the external forces acting on the system when the system is displaced through a virtual displacement δa_1 is

$$\delta W=-\pi\rho VF_e\cos\bar{\alpha}\int_0^L\delta a_1c\dot{a}_1h_1^2(y)dy+F_0\delta a_1h_1(y_c)\cos\bar{\alpha}$$

The generalized force is then

$$Q=\frac{\delta W}{\delta a_1}$$

$$=-\pi\rho V\dot{a}_1F_e\cos\bar{\alpha}\int_0^L c[h_1(y)]^2dy+F_0h_1(y_c)\cos\bar{\alpha}$$

The aerodynamic forces associated with acceleration and displacement have been ignored in this development. The experimental technique, however, accounts for these forces in that the measured natural frequency for each condition was used in reducing the data. By use of Lagrange's equation of motion (ref. 18) it can be shown that

$$M_e\ddot{a}_1+(C_e+C_a)\dot{a}_1+K_ea_1=F_0h_1(y_c)\cos\bar{\alpha}$$

where

$$C_a=\pi\rho VF_e\cos\bar{\alpha}\int_0^L c[h_1(y)]^2dy$$

It is desirable to determine the ratio of aerodynamic damping to critical damping of the system. Critical

damping is defined as

$$C_{cr}=2\sqrt{K_e M_e}$$

Since

$$M_e\omega_1^2=K_e$$

then

$$C_{cr}=2\omega_1 M_e$$

and

$$\frac{C_a}{C_{cr}}=\frac{\pi\rho V F_e \cos\bar{\alpha}\int_0^L c[h_1(y)]^2dy}{2\omega_1 M_e}$$

This expression may be rearranged to solve for a more general nondimensional aerodynamic-damping coefficient F_e

$$F_e=\frac{\frac{C_a}{C_{cr}}2\omega_1 M_e}{\pi\rho V\cos\bar{\alpha}\int_0^L c[h_1(y)]^2dy}$$

and in terms of conventional flutter parameters

$$F_e=\frac{k\frac{C_a}{C_{cr}}}{\kappa_e\cos\bar{\alpha}}$$

where

$$k=\frac{\omega_1 c_r}{2V}$$

and

$$\kappa_e=\frac{\pi\rho c_r\int_0^L c[h_1(y)]^2dy}{M_e}$$

In order to solve for either $\frac{C_a}{C_{cr}}$ or F_e, the natural frequency ω_1 and the generalized mass M_e must be known.

As mentioned previously, ω_1 was determined experimentally at each test condition—a procedure which automatically accounts for aerodynamic-stiffness effects. The generalized mass of the system was also determined experimentally by measuring the change in natural frequency produced by attaching a known concentrated mass to the shaker coil. The natural frequency of the system without the additional mass is

$$\omega_1^2=\frac{K_e}{M_e}$$

and the natural frequency of the system with the added mass is

$$\omega_{1_\Delta}^2=\frac{K_e}{M_e+\Delta M_c[h_1(y_c)\cos\bar{\alpha}]^2}$$

where ΔM_c is the added mass. From these expressions for the natural frequency, it follows that

$$M_e=\frac{\Delta M_c[h_1(y_c)\cos\bar{\alpha}]^2}{\frac{\omega_1^2}{\omega_{1_\Delta}^2}-1}$$

Since the determinations of M_e were made in still air rather than in a vacuum, the values of generalized mass obtained would correctly include the apparent mass of the air surrounding the wing.

REFERENCES

1. Sisto, Fernando: Stall-Flutter in Cascades. Preprint No. 402, S.M.F. Pub. Fund Preprint, Inst. Aero. Sci., Jan. 1953.
2. Schnittger, Jan R.: The Stress Problem of Vibrating Compressor Blades. Jour. Appl. Mech., vol. 22, no. 1, Mar. 1955, pp. 57–64.
3. George, M. Baron T.: A Theoretical Approach to the Problem of Stall Flutter. Contract AF 33(038)–21406, Cornell Univ. Graduate School of Aero. Eng., Aug. 15, 1953.
4. Jones, W. P.: Aerofoil Oscillations at High Mean Incidences. R. & M. No. 2654, British A.R.C., Apr. 1948.
5. Liepmann, H. W.: On the Application of Statistical Concepts to the Buffeting Problem. Jour. Aero. Sci., vol. 19, no. 12, Dec. 1952, pp. 793–800, 822.
6. Liepmann, H. W.: Parameters for Use in Buffeting Flight Tests. Rep. No. SM–14631, Douglas Aircraft Co., Inc., Jan. 3, 1953.
7. Miles, John W.: An Approach to the Buffeting of Aircraft Structures by Jets. Rep. No. SM–14795, Douglas Aircraft Co., Inc., June 1953.
8. Huston, Wilber B., and Skopinski, T. H.: Measurement and Analysis of Wing and Tail Buffeting Loads on a Fighter Airplane. NACA Rep. 1219, 1955. (Supersedes NACA TN 3080.)
9. Runyan, Harry L., Woolston, Donald S., and Rainey, A. Gerald: Theoretical and Experimental Investigation of the Effect of Tunnel Walls on the Forces on an Oscillating Airfoil in Two-Dimensional Subsonic Compressible Flow. NACA Rep. 1262, 1956. (Supersedes NACA TN 3416.)
10. Patterson, John L.: A Miniature Electrical Pressure Gage Utilizing a Stretched Flat Diaphragm. NACA TN 2659, 1952.
11. Helfer, Arleigh P.: Electrical Pressure Integrator. NACA TN 2607, 1952.
12. Scrafford, Robert L.: An Electronic Phasemeter for the Testing of Servomechanisms. Rep. No. ID–683–S–1, Cornell Aero. Lab., Inc., Apr. 14, 1950.
13. Timman, R., Van de Vooren, A. I., and Greidanus, J. H.: Aerodynamic Coefficients of an Oscillating Airfoil in Two-Dimensional Subsonic Flow. Jour. Aero. Sci., vol. 18, no. 12, Dec. 1951, pp. 797–802, 834.
14. Halfman, Robert L., Johnson, H. C., and Haley, S. M.: Evaluation of High-Angle-of-Attack Aerodynamic-Derivative Data and Stall-Flutter Prediction Techniques. NACA TN 2533, 1951.
15. Bratt, J. B., and Wight, K. C.: The Effect of Mean Incidence, Amplitude of Oscillation, Profile, and Aspect Ratio on Pitching Moment Derivatives. R. & M. No. 2064, British A.R.C., 1945.
16. Herr, Robert W.: Preliminary Experimental Investigation of Flutter Characteristics of M and W Wings. NACA RM L51E31, 1951.
17. Theodorsen, Theodore: General Theory of Aerodynamic Instability and the Mechanism of Flutter. NACA Rep. 496, 1935.
18. Scanlan, Robert H., and Rosenbaum, Robert: Introduction to the Study of Aircraft Vibration and Flutter. The Macmillan Co., 1951.